Contents lists available at ScienceDirect

Neurobiology of Disease

ELSEVIER

Characterization of seipin/BSCL2, a protein associated with spastic paraplegia 17

Daisuke Ito [a,*], Taishi Fujisawa [a], Hiroshi Iida [b], Norihiro Suzuki [a]

[a]Department of Neurology, School of Medicine, Keio University, 35 Shinanomachi, Shinjuku-ku, Tokyo 160-8582, Japan
[b]Laboratory of Zoology, Graduate School of Agriculture, Kyushu University, Higashiku Hakozaki 6-10-1, Fukuoka 812-8581, Japan

ARTICLE INFO

ABSTRACT

Seipin, which is encoded by the BSCL2 gene, is a glycoprotein of unknown biochemical function that is associated with dominant hereditary motor neuron diseases. Mutations in the N-glycosylation site of seipin are associated with the disease states and result in accumulation of unfolded protein in the endoplasmic reticulum (ER), leading to the unfolded protein response (UPR) and cell death, suggesting that these diseases are tightly associated with ER stress. Here, we determined the subcellular localization, functional domains, and distribution of seipin in tissues. Our studies show that the transmembrane domains in seipin are critical for ER retention, ubiquitination, formation of inclusions, and activation of UPR. Using immunohistochemistry, seipin expression is detected in neurons in the spinal cord and in the frontal lobe cortex of the brain. The present study provides new insights into the biology of seipin protein that should help our understanding of the pathogenesis of seipin-related diseases.

© 2008 Elsevier Inc. All rights reserved.

Introduction

Heterozygosity for mutations in the *seipin/BSCL2* gene (namely, the N88S and S90L mutations) is associated with the autosomal dominant motor neuron diseases, Silver syndrome/spastic paraplegia 17 (SPG17) and distal hereditary motor neuropathy type V (dHMNV) (Windpassinger et al., 2004). Recent analyses of the clinical phenotypes caused by the N88S and S90L mutations have revealed a wide spectrum of defects in motor neurons, with both upper and lower motor neurons variously affected (Auer-Grumbach et al., 2005; Irobi et al., 2004). Based on the available evidence, we proposed that seipin-related motor neuron diseases should be referred to collectively as "seipinopathies" (Ito and Suzuki, 2007b). The *seipin* gene was first identified as a candidate for congenital generalized lipodystrophy type 2 (CGL2) (Agarwal et al., 2002). Individuals homozygous for null mutations in *seipin* have severe lipoatrophy and mental retardation but not abnormality of the motor neurons (Agarwal and Garg, 2003, 2004; Fu et al., 2004). By contrast, lipodystrophy and metabolic disturbances are not reported in seipinopathies (Auer-Grumbach et al., 2005; Irobi et al., 2004). Although the biochemical function(s) of seipin is not well understood, it has been speculated that the mutation in *seipin* associated with CGL2 is a loss-of-function mutation, whereas gain-of-function mutations in *seipin* (N88S, S90L) lead to seipinopathy (Agarwal and Garg, 2004; Ito and Suzuki, 2007b).

We recently showed that the N88S and S90L mutant forms of seipin disrupt the N-glycosylation motif, enhance ubiquitination, form inclu-

sion bodies, and appear to be improperly folded, leading to accumulation of the mutant protein in the endoplasmic reticulum (ER). We also showed that expression of the mutant proteins in cultured cells activates the UPR pathway and induces cell death, suggesting that seipinopathy is tightly associated with ER stress (Ito and Suzuki, 2007a).

Several points remain to be elucidated, however, in order to clarify the molecular pathogenesis of seipinopathies. First, it would be helpful to learn more about the structure and biochemical function of seipin. A recent study (Lundin et al., 2006) suggests that seipin has two transmembrane domains and that both termini face the cytosol. However, little information is available regarding secondary structure and functional domains of seipin. Second, it should be interesting to learn about the distribution of seipin in various tissues, as high levels of expression are detected in the brain and testis by RNA blotting but a detailed study of expression has not previously been reported. And third, it should be interesting to determine what types of inclusions (if any) form in cells that express mutant seipin. Over-expression of several proteins associated with neurodegeneration, such as polyglutamine and α-synuclein, can lead to formation of ubiquitinated inclusions, termed aggresomes (Garcia-Mata et al., 1999; Johnston et al., 1998; Junn et al., 2002; Kopito, 2000; Lee and Lee, 2002; Mishra et al., 2003; Muqit et al., 2004; Tanaka et al., 2004; Tran and Miller, 1999; Waelter et al., 2001), which may be either cytotoxic or cytoprotective (Arrasate et al., 2004; DiFiglia et al., 1997; Klement et al., 1998; Orr, 2004; Saudou et al., 1998; Sisodia, 1998; Taylor et al., 2003). Whether or not seipin inclusions have the same characteristics as the well-studied aggresomes has not previously been addressed.

Here, we focused on the biochemical properties and distribution of seipin. Our results show that the transmembrane domains of seipin are required for its retention in the ER, formation of inclusions, and

* Corresponding author. Fax: +81 3 3353 1272.
E-mail address: d-ito@jk9.so-net.ne.jp (D. Ito).

Available online on ScienceDirect (www.sciencedirect.com).

activation of UPR. Seipin inclusion bodies in transfected cells have unique characteristics and appear to be distinct from aggresomes such as huntingtin aggresomes. Immunohistochemistry reveals that seipin is expressed in the nervous system, pituitary gland, and testis. The results point to possible functions of seipin that should lead to new insights into treatment of seipin-related diseases.

Materials and methods

Cell culture and reagents

The Neuro 2a mouse neuroblastoma (N2a) and HeLa human carcinoma cells were maintained in Dulbecco's modified Eagle's medium (Gibco, Grand Island, NY) containing 10% fetal bovine serum. Transfections were done with Lipofectamine Plus reagent (Invitrogen, Carlsbad, CA) according to the manufacturer's instructions.

cDNAs

Based on alignment of protein sequences from several species, the putative seipin open reading frame contains two possible start codons, the use of which is predicted to result in production of proteins 398 or 462 amino acids in length (Agarwal and Garg, 2004). Recently, Lundin et al. showed that the predominant form of seipin is 462 amino acids and thus, we numbered the residues accordingly in Fig. 2. Plasmids used to express wild-type and mutant forms of human seipin were described previously (Ito and Suzuki, 2007a). Deletion forms of seipin, ΔNT, ΔCT, ΔTm2, ΔTm1–2, and ΔLoop, were generated using appropriate restriction enzymes and T4 polymerase. The deletion constructs ΔTm1 and ΔTm1+2 were generated by PCR-based mutagenesis using the primers 5′-ATATGCTGCAGTATTCCTATATGCCG and 5′-CACCCGAT-CACGTCCACCCT. Plasmids supplying HA-tagged human ubiquitin (Hatakeyama et al., 2001), dog calnexin (CNX)(Wada et al., 1994), and EGFPN1-tNhtt-60Q (Wang et al., 1999) were kindly provided by Dr. Shigetsugu Hatakeyama (Hokkaido University Graduate School of Medicine, Sapporo, Japan), Dr. Ikuo Wada (Fukushima Medical University, Fukushima, Japan), and Dr. Arifumi Kosakai (Keio University, Tokyo, Japan), respectively.

Antibodies

A rabbit polyclonal antiserum that recognizes human seipin (SCT14) was described previously (Ito and Suzuki, 2007a). Mouse monoclonal anti-KDEL, anti-Hsp70/Hsc70 (SPA-820), rabbit polyclonal anti-CNX NH2 terminus (SPA-865), and anti-CNX COOH terminus (SPA-860) were purchased from Stressgen (San Diego, CA). The 9E10 (anti-myc) and anti-ubiquitin (P4D1) mouse monoclonals were purchased from Santa Cruz Biotechnology (Santa Cruz, CA). Mouse monoclonal anti-β actin, anti-α tubulin, and anit-V5 were from Invitrogen (Carlsbad, CA). Mouse monoclonal anti-His (clone HIS-1), anti-vimentin (clone V9), and anti-Golgi 58K (clone 58K-9) were from Sigma (St. Louis, MO). Mouse monoclonal anti-HA (clone 12CA5) was from Roche (Basel, Switzerland). Rabbit polyclonal anti-myc and mouse monoclonal anti-Na+/K+ATPase α-1 (C464.6) were from Upstate Biotechnology (Lake Placid, NY). Mouse monoclonal anti-poly-ubiquitin antibody (FK2) was from Nippon Bio-Test Lab. (Tokyo, Japan); mouse monoclonal anti-cyclooxygenase IV (COX-IV) was from Molecular Probes (Eugene, OR). Rabbit polyclonal anti-pericentrin and anit-GRP78 (Bip) were from Abcam (Cambridge, U.K.). Rabbit polyclonal anti-giantin was from Covance (San Diego, CA). And mouse monoclonal anti-ACTH was from Chemicon (Temecula, CA).

Immunoblot analysis

Cells were briefly sonicated in cold lysis buffer (50 mM Tris–HCl, pH 7.4, 150 mM NaCl, 0.5% NP-40, 0.5% sodium deoxycholate, 0.25% sodium dodecyl sulfate, 5 mM EDTA and protease inhibitor cocktail

from Sigma). The total protein concentration in the supernatant was determined using a Bio-Rad protein assay kit. Then, proteins were analyzed by immunoblotting as follows. Protein samples were separated by reducing SDS-PAGE on a 4% to 20% Tris–glycine gradient gel (Invitrogen), after which proteins were transferred to a polyvinylidene difluoride membrane (Millipore, Billerica, MA). The membrane was incubated with primary antibodies (anti-KDEL, 1:2500; anti-Golgi 58K, 1:7500; anti-Na+/K+ATPase α-1, 1:7500; anti anti-COX-IV, 1:1000; anti-β-actin, 1:1000; anti-α-tubulin, 1:1000; anti-V5, 1:1000; anti-CNX NH2 terminus, 1:1000; anti-CNX COOH terminus, 1:1000; SCT14 antiserum, 1:500; or anti-CHOP, 1:1000) followed by incubation with horseradish peroxidase-conjugated secondary antibodies and detection using enhanced chemiluminescence reagents as described by the supplier (PerkinElmer Life Sciences, Boston, MA). Protein levels were determined by densitometry using an Epson ES-2000 scanner (Tokyo, Japan) and Image J (National Institutes of Health, Bethesda, MD).

Subcellular fractionation analysis

Subconfluent N2a cells grown in 60 mm dishes were homogenized in 1 ml of ice-cold sucrose buffer (0.25 M sucrose, 1 mM EDTA, 20 mM HEPES–NaOH, pH 7.4, and a mixture of protease inhibitors) by passing the cells 10 times through a 26-gauge needle. Lysates were cleared by centrifugation at 800 ×g for 15 min. The supernatants were overlaid on a step gradient consisting of 1 ml each of 30, 20, 17.5, 15, 12.5, 10, 7.5, 5 and 2.5% (v/v) Iodixanol (OptiPrep reagent, Axis-Shield Oslo, Norway) in homogenization buffer. After centrifugation for 2.5 h at 200,000 ×g (SW40 rotor, Beckman, München, Germany), nine fractions were collected from the top of the gradient. After TCA precipitation, each fraction was analyzed by immunoblotting using 9E10 and anti-KDEL, Golgi 58K, Na+/K+ATPase α-1 and COX-IV antibodies.

Proteinase K protection assay

At 48 h post-transfection, N2a cells expressing exogenous wild-type or mutant seipin cDNAs were lysed in ice-cold buffer containing 10 mM Tris–HCl, pH 7.4, 0.25 M sucrose, 1 mM MgCl2 by passing cells repeatedly through a 26-gauge needle. Lysates were cleared by centrifugation at 1000 ×g for 10 min. The supernatant was exposed to proteinase K (1 or 10 μg/ml) for 20 min at room temperature and subsequently separated by 10–20% Tris–glycine (Invitrogen) SDS-PAGE and analyzed by immunoblotting.

Immunofluorescence detection

HeLa cells grown on coated coverslips were transfected with the appropriate expression plasmids. After 48 h, cells were fixed with 4% paraformaldehyde at room temperature for 10 min and then permeabilized in 0.2% Triton X-100 for 5 min. After blocking of nonspecific binding, coverslips were incubated with 1:500 polyclonal anti-myc antibody, 1:1000 9E10 antibody, 1:1000 anti-V5 or 1:500 SCT14 antiserum along with organelle marker antibodies (1:1000 anti-GRP78, 1:100 anti-Hsp70/Hsc70, 1:100 anti-ubiquitin, 1:75 anti-vimentin, 1:500 anti-pericentrin, or 1:240 anti-poly-ubiquitin) diluted in PBS, 0.2% Tween-20, 3% bovine serum albumin. After three washes, the coverslips were incubated with fluorescein isothiocyanate-conjugated anti-rabbit and Texas Red-conjugated anti-mouse secondary antibodies, and then mounted. Immunofluorescent staining was examined using a LSM 5 Pascal confocal microscope (Carl Zeiss, Oberkochen, Germany).

Immunohistochemical detection of seipin

Paraffin sections of human frontal lobe (female aged 82 years) and spinal cord (male aged 36 years) were purchased from Biochain (CA,

D. Ito et al. / Neurobiology of Disease 31 (2008) 266–277

USA). Spinal cord sections from a patient with amyotrophic lateral sclerosis (ALS) were kindly provided by Dr. Masaki Takao (Department of Cognitive and Intractable Neurological Disorders, Mihara Memorial Hospital) and Dr. Katsuhisa Ogata (Department of Neurology, Higashisaitama Hospital, National Hospital Organization). Paraffin was removed from the sections with xylene followed by hydration in an ethanol series. The sections were treated with boiling 10 mM Citrate Buffer (pH 6.0) and then incubated with 0.05% saponin for 30 min at room temperature in preparation for immunohistochemistry.

Before isolation and staining of mouse tissues was conducted, the protocol was approved as meeting the Animal Experimentation Guidelines of Keio University School of Medicine. Tissues collected from male C57/BL6 mice (pituitary gland) or ddy mice (testis) were fixed by perfusion with PBS, 4% paraformaldehyde. The tissue samples were subsequently removed, rapidly frozen in dry ice powder or liquid nitrogen, and sliced using a cryostat. Immunohistochemistry was performed essentially as described previously (Iida et al., 2006; Ito et al., 1998, 1999, 2001a,b) using SCT14 antiserum or the pre-immune serum (1:1000) along with a mouse anti-ACTH monoclonal antibody (1:500). Immunostained spinal cord, cerebrum or pituitary gland sections were counterstained with the DNA dye Hoechst 33342 (Molecular Probes, Eugene, OR) and the testis sample was counterstained with the DNA dye SYTOX Green (Molecular probes)(Iida et al., 2006).

Statistical analysis

Statistical analysis of the data was performed by one-way ANOVA with Fisher's protected least significant difference test using Statview 5.0 (Statview, Berkley, CA).

Results

Seipin is an ER membrane-resident protein

By confocal immunofluorescence microscopy, seipin is primarily detected in the ER (Ito and Suzuki, 2007a; Windpassinger et al., 2004). To further analyze the subcellular distribution of seipin, here we performed density subcellular fractionation in N2a cells that express seipin. The distributions of both wild-type and N88S mutant seipin were compared
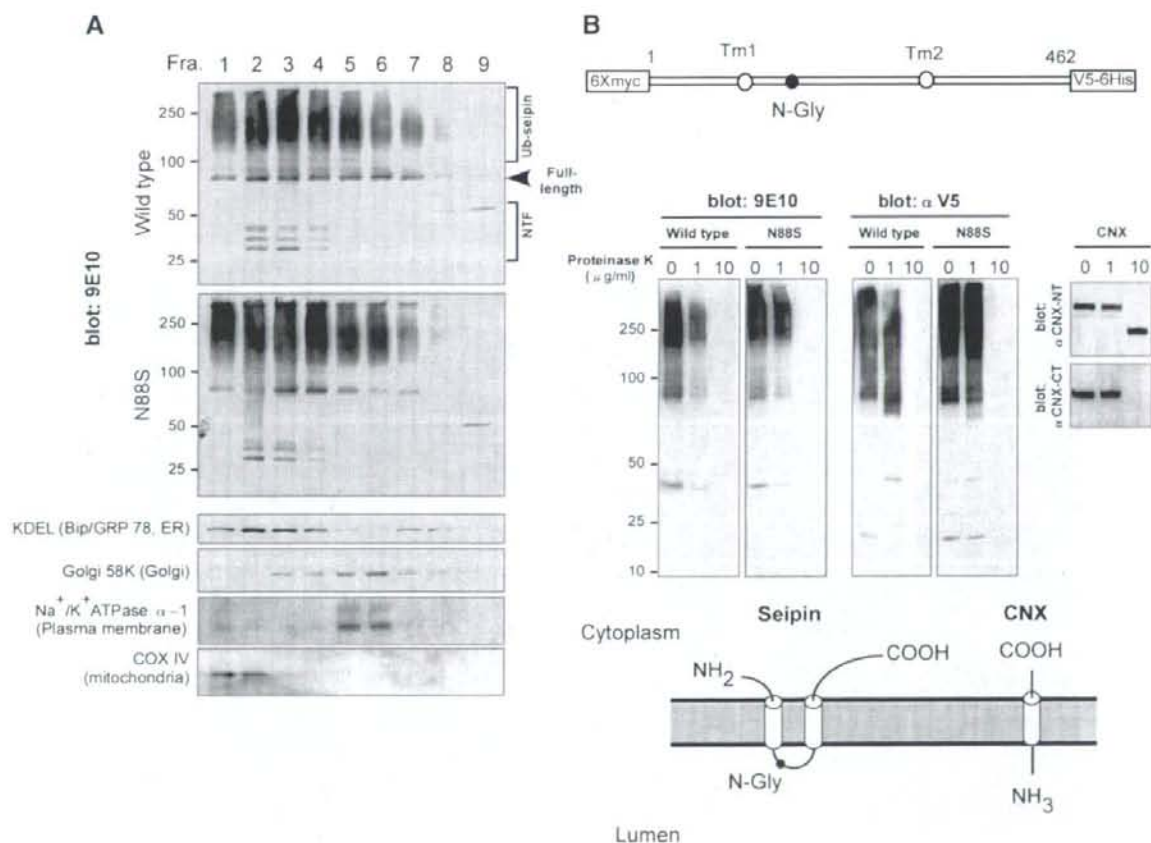

Fig. 1. Subcellular fractionation of seipin. (A) Sucrose density gradient analysis. Subconfluent N2a cells exogenously expressing wild-type or mutant (N88S) seipin (60 mm dishes) were lysed and were fractionated by velocity sedimentation. Fractions were analyzed by immunoblotting using 9E10, anti-KDEL (78 kDa protein, Bip/GRP78, as an ER marker), anti-Golgi 58K (a Golgi marker), anti-Na+/K+ATPase α-1 (a plasma membrane marker), and anti-COX-IV (a mitochondrial marker). Note that both wild-type and mutant seipins are predominantly detected in ER fractions. Ub-seipin, ubiquitinated seipin; NTF, N-terminal fragments. (B) N2a cells were transfected with plasmids for expression of wild-type or mutant seipin tagged with the c-myc epitope at the NH2 terminus and V5 at the COOH terminus, and with dog CNX. Post-nuclear supernatant from transfected cells was incubated with increasing amounts of Proteinase K (0, 1 and 10 µg/ml) for 20 min at room temperature. Immunoblotting was performed using anti-myc (9E10), anti-V5, anti-NH2 terminus of CNX (αCNX-NT), and anti-CNX COOH terminus (αCNX-CT) antibodies. Proteinase K treatment resulted in complete degradation of the NH2 and COOH termini of seipin. N-Gly, N-glycosylation site.
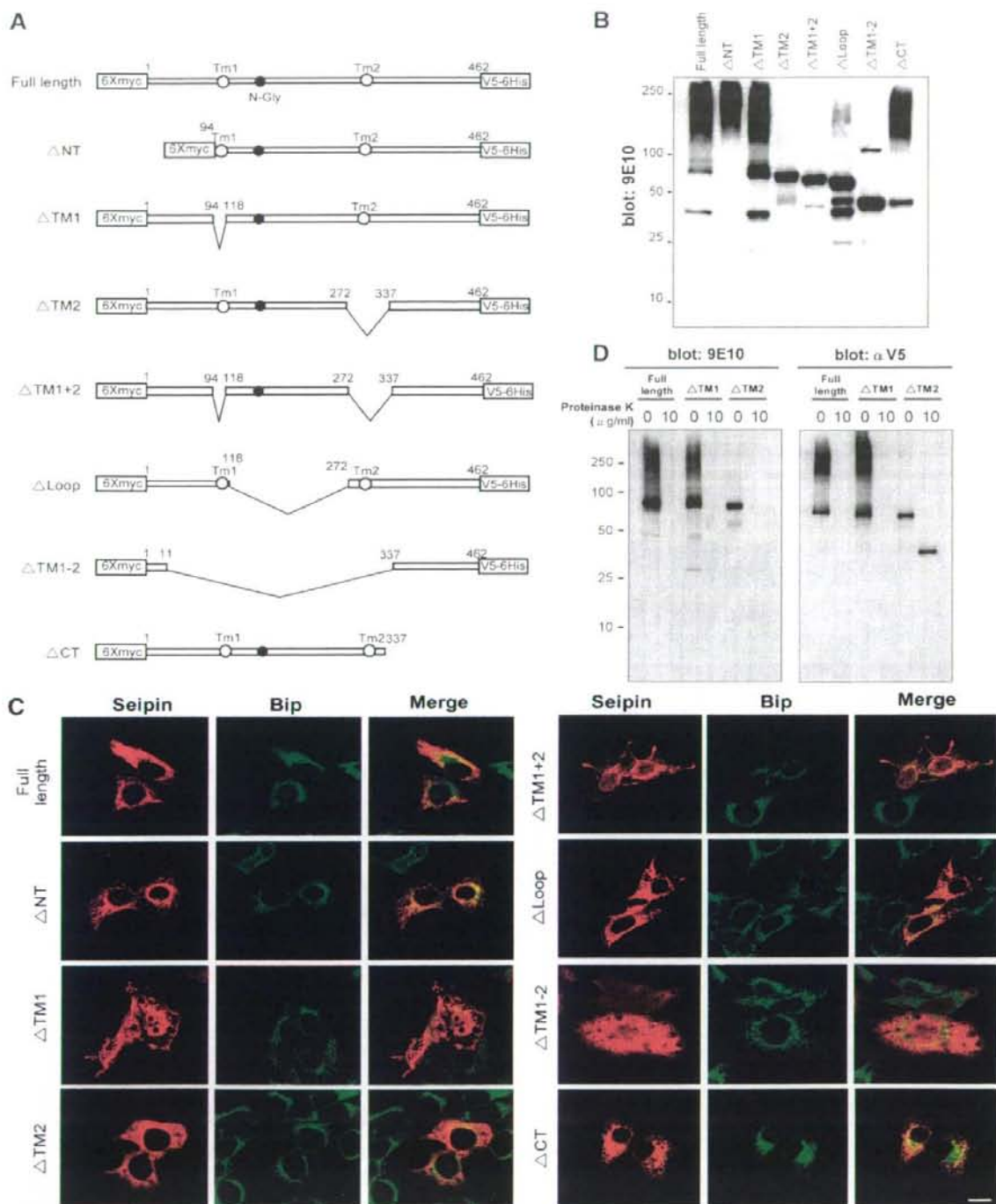
Fig. 2. Effects of deleting specific domains of seipin on ubiquitination and subcellular localization. (A) Schematic diagram showing the location of deletions introduced into seipin. All seipin constructs contain a myc tag at the NH2 terminus and a V5 tag at the COOH terminus. (B) Immunoblot analysis of seipin deletion constructs expressed in HeLa cells and detected using anti-myc (9E10). A total of 10 μg of protein per lane was loaded on a 4–20% Tris–glycine gradient gel. (C) Intracellular localization of full-length and deleted forms of seipin in HeLa cells. HeLa cells transfected with each of a series of deletion constructs were grown on coverslips and fixed with 4% paraformaldehyde, permeabilized with 0.2% Triton X-100, and double-labeled with 9E10 (red) and anti-GRP 78 (BiP, an ER maker; green) antibodies. Note that all forms of seipin lacking the first transmembrane domain (ΔTm1, ΔTm1+2, ΔTm1−2) failed to localize to the ER. Scale bar indicates 10 μm. (D) A proteinase K protection assay on N2a cells expressing full-length seipin, ΔTm1 or ΔTm2. Post-nuclear cell supernatant was incubated without or with Proteinase K (10 μg/ml) for 20 min at room temperature. Both termini of full-length seipin and of ΔTm1, and the NH2-terminus of ΔTm2, were fully degraded, whereas the C-terminus of ΔTm2 was protected.
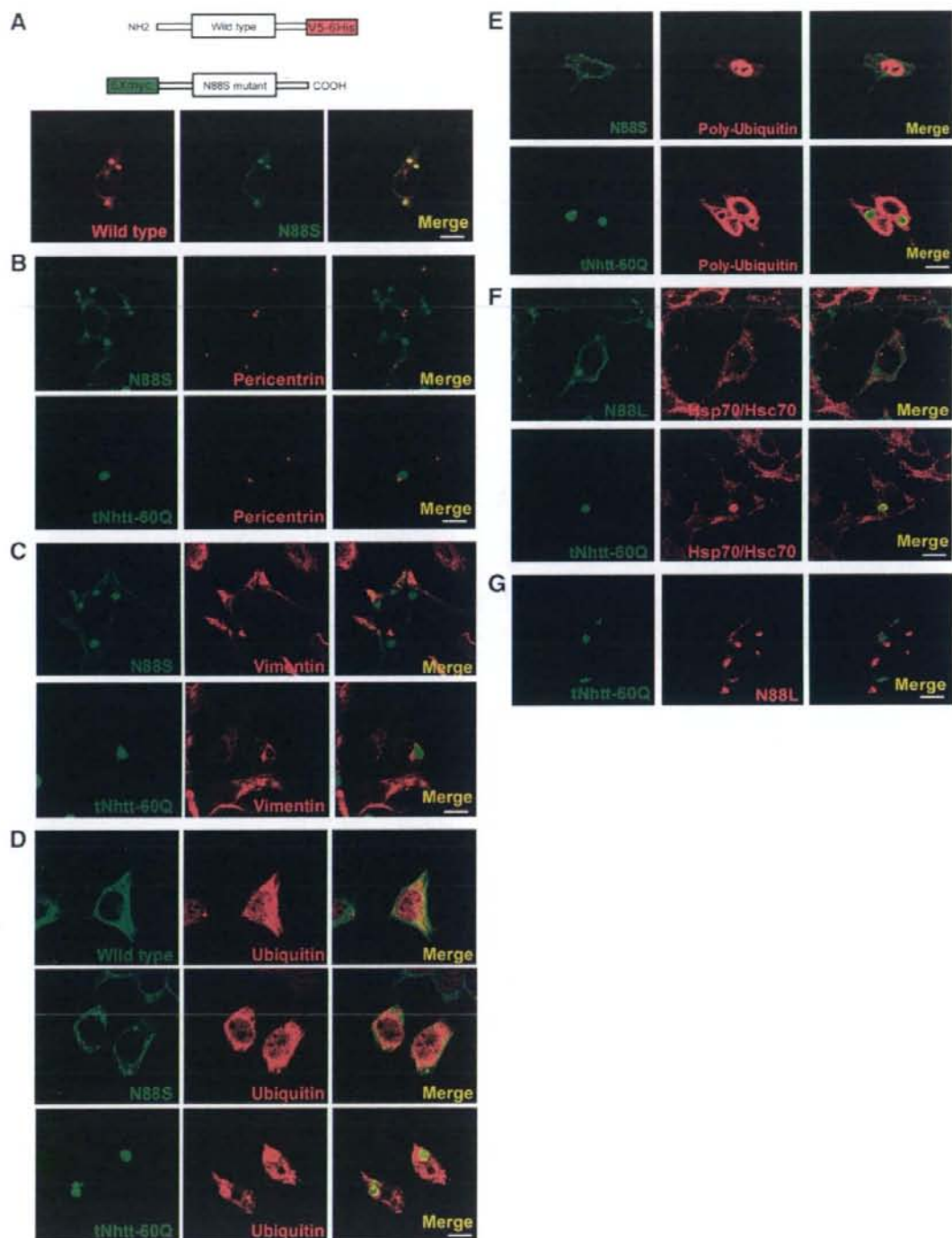
Fig. 3. Characterization of seipin inclusion bodies. (A) HeLa cells were transiently transfected with wild-type seipin tagged with V5 at the COOH terminus and N88S mutant seipin tagged with myc at the NH2 terminus. Two days post-transfection, cells were fixed and inclusion bodies were co-labeled with polyclonal anti-myc (green) and monoclonal anti-V5 antibody (red). Note that both wild-type and mutant seipin assemble at the inclusion body. (B–F), cells expressing myc-tagged wild-type, mutant seipin or EGFPN1-tNhtt-60Q were double-labeled with polyclonal anti-myc antibody or monoclonal anti-myc (9E10) and anti-pericentrin (B), vimentin (C), ubiquitin (D), poly-ubiquitin (E), or Hsp70/Hsc70 (F) antibody. (G) HeLa cells co-transfected with N88S mutant seipin tagged with myc at the NH2 terminus and with EGFPN1-tNhtt-60Q, and subsequently labeled with 9E10 (red). Note that mutant seipin is never recruited to the tNhtt-60Q-aggresome. Scale bar indicates 10 μm.

271

with the distributions of markers for various subcellular compartments: BiP (an ER marker), Golgi 58K (Golgi), Na+/K+/ATPase α-1 (plasma membrane) and COX-IV (mitochondria).

Immunoblot analysis using the 9E10 anti-myc antibody reveals bands consistent with a ubiquitinated high molecular complex, the full-length 6Xmyc-seipin-His (~78 kDa) and N-terminal fragments of seipin (35-to 48-kDa) as described in our previous report (Fig. 1A and Ito and Suzuki, 2007a). The electromobility of full-length 6Xmyc-seipin-His is higher than predicted based on the amino acid sequence (~78 kDa observed versus ~67 kDa predicted), consistent with a previous report (Ito and Suzuki, 2007a; Windpassinger et al., 2004). Moreover, as expected we found that seipin, including most N-terminal fragments of seipin, is predominantly detected in subcellular fractions enriched for the ER-resident protein BiP (Fig. 1A). This pattern of distribution was the same for N2a cells expressing the N88S mutant form of seipin, suggesting that this mutation in the N-glycosylation site of seipin does not affect localization.

Based on analysis using a hidden Markov model method (http://www.cbs.dtu.dk/services/TMHMM/), human seipin is thought to be a membrane protein with two transmembrane domains. Recently, Lundin et al. engineered glycosylation sites at both ends of seipin and used the resulting protein to assess seipin topology (Lundin et al., 2006). They found that the NH2 and COOH termini of seipin were not N-linked glycosylated after expression using an in vitro transcription/translation system, suggesting that both termini face the cytosol. In this study, we sought to use a proteinase K protection assay to assay the topology of seipin directly.

To do this, wild-type and N88S mutant seipin tagged with c-myc and V5 epitopes at the NH2 and COOH termini, respectively, were first transfected into N2a cells. CNX, a type I transmembrane protein in the ER, was monitored as a control. The cell lysates were homogenized with a 26-gauge needle syringe to ensure minimal disruption of organelle integrity, digested with proteinase K, and then subject to immunoblotting with antibodies specific for the myc- or V5-epitope tags. As shown in Fig. 1B, both the NH2 and the COOH terminus of human seipin were easily digested by proteinase K, as was the COOH terminus of CNX, which faces the cytoplasm. In contrast, proteinase K was not able to digest the NH2 terminus of CNX, which is known to face the lumenal side of the membrane. Mutant seipin had the same pattern of protease sensitivity as the wild-type form. The asparagine residue (88) that is affected in the mutant protein is known to be N-glycosylated in the ER lumen (Ito and Suzuki, 2007a; Lundin et al., 2006; Windpassinger et al., 2004) and thus, it seems reasonable to propose that it is located on the lumenal loop domain. Based on these results, we conclude that seipin has two transmembrane domains and additionally, that for both the wild-type and mutant forms, both termini of seipin face the cytosol rather than the ER lumen, consistent with a previous report (Lundin et al., 2006).

The first transmembrane domain of seipin is essential for retention in the ER

We next sought to determine what region(s) of seipin are required for its localization to the ER. To do this, we constructed a series of deletion constructs and assayed their subcellular localization in HeLa cells, which are big enough for subcellular localization studies (Fig. 2A). When cells are transiently transfected with constructs in which the NH2 terminus, the COOH terminus, the loop region, or the first transmembrane domain has been deleted (ΔNT, ΔTm1, ΔLoop, ΔCT), some portion of the resultant proteins are detected on an immunoblot as high molecular weight complexes, consistent with ubiquitination (Ito and Suzuki, 2007a). However, the high molecular weight signal is not present in protein extracts from cells that express a wild-type or N88S mutant construct in which the second transmembrane domain has been deleted (Fig. 2B, wild-type ΔTm2, ΔTm1+2, ΔTm1−2 and data not shown for N88S).

The results of confocal microscopy (Fig. 2C) make it clear that the NH2-, COOH-terminal and second transmembrane domain deleted forms of seipin (ΔNT, ΔCT, ΔTm2) show a typical reticular pattern in the cytoplasm, indicating that these are mainly in the ER. In contrast, for seipin proteins lacking the first transmembrane domain (ΔTm1 or ΔTm1+2), a portion of the protein is localized to the ER but these forms are also detectable in the cell periphery and nucleus. Moreover, ΔTm1−2 seipin is diffuse in the cell body. Taken together, the data suggest that the first transmembrane domain of seipin is critical for ER retention. Furthermore, the results of a protease K protection assay using the transmembrane domain deletion proteins as substrates reveals that the NH2 terminus of ΔTm2 is easily digested by proteinase K, whereas the COOH terminus is resistant (Fig. 2D). In contrast, both termini of ΔTm1 were fully digested by proteinase K. As ER membrane retention is affected for the ΔTm1 protein, we conclude that all of the ΔTm1 protein is exposed to the cytosol and thus, can easily be degraded by the proteinase.

Characterization of inclusion bodies in cells expressing a mutant form of seipin

In a previous paper (Ito and Suzuki, 2007a), we demonstrated that neuronal and non-neuronal cells expressing the N88S and S90L mutant proteins contain inclusion bodies, which are rarely detected in wild-type cells. To characterize the inclusion bodies, we compared inclusions formed in the presence of wild-type and mutant seipin. HeLa cells were transfected with wild-type seipin harboring a V5 epitope tag at the COOH terminus and mutant seipin with the c-myc epitope tag at the NH2 terminus. The cells were then examined immunocytochemically and using confocal microscopy. Interestingly, the wild-type and mutant seipin co-localize in inclusions (Fig. 3A), suggesting that the mutant form of the protein may recruit the wild-type form to inclusion bodies.

Expression of mutant proteins associated with neurodegenerative diseases, such as huntingtin, parkin, α-synuclein, and prion proteins, leads to formation of ubiquitinated aggregates termed aggresomes (Garcia-Mata et al., 1999; Johnston et al., 1998; Junn et al., 2002; Kopito, 2000; Lee and Lee, 2002; Mishra et al., 2003; Muqit et al., 2004; Tanaka et al., 2004; Tran and Miller, 1999; Waelter et al., 2001) that have been well-characterized biochemically. A characteristic feature of aggresomes is that they form at the microtubule organizing centre (MTOC). This is consistent with the finding that misfolded proteins are commonly transported along microtubules and then assembled in and around the MTOC (Johnston et al., 1998; Junn et al., 2002; Kopito, 2000; Tanaka et al., 2004). Another characteristic of aggresomes is deposition of intermediate filaments such as vimentin, which often forms a cage-like structure around inclusions (Johnston et al., 1998; Junn et al., 2002; Kopito, 2000). Aggresomes are primarily made up of chaperones, Hsp70 and Hsc40 protein, ubiquitin, 19S and 26S proteasome subunits (Garcia-Mata et al., 1999; Junn et al., 2002; Kalchman et al., 1996; Sieradzan et al., 1999; Tanaka et al., 2004). In order to ask how similar seipin inclusions are to aggresomes, we compared seipin inclusions in several ways to the well-examined aggresomes of huntingtin.

To examine the relationship between seipin inclusions and the MTOC, we first compared the distribution of seipin inclusions to that of pericentrin, an MTOC marker protein. As a control for aggresome formation, we expressed an NH2-terminal fragment of huntingtin with an expanded 60 CAG repeat (EGFPN1-tNhtt-60Q) in cells (Wang et al., 1999). Aggresomes are reportedly targeted to and congregate specifically at the MTOC (Fig. 3B). In contrast to aggresomes, we found that seipin inclusions are not localized near the MTOC, suggesting that the inclusions form via a different mechanism.

Next we compared the distribution of the intermediate filament protein vimentin in cells with huntingtin aggresomes to its distribution

D. Ito et al. / Neurobiology of Disease 31 (2008) 266–277

in cells with seipin inclusions. In the aggresome-containing cells, vimentin formed a ring-like halo surrounding the core of the aggresome, consistent with previously reported results (Fig. 3C) (Johnston et al., 1998; Junn et al., 2002; Kopito, 2000). In contrast (upper panel, Fig. 3C), the distribution of vimentin appears to be unaffected in cells that express seipin and form seipin inclusions.

We also compared the distribution of seipin inclusions to that of major protein components of aggresomes; namely, ubiquitin and the major cytosolic/nucleic molecular chaperon Hsp70. The results of a previous study in our lab indicate that seipin is ubiquitinated (Ito and Suzuki, 2007a). In this work, we co-expressed seipin and ubiquitin and found that the distribution of wild-type and mutant seipin overlaps with that of ubiquitin in cell bodies (Fig. 3D). Unexpectedly, however, we could not detect ubiquitin in seipin inclusions to any significant level. Moreover, the results were the same when we tested a different antibody (anti-poly-ubiquitin) in cells expressing seipin alone (Fig. 3E), whereas consistent with previous reports (Garcia-Mata et

al., 1999; Junn et al., 2002; Kalchman et al., 1996; Sieradzan et al., 1999; Tanaka et al., 2004), ubiquitin was readily detected in tNhtt-60Q aggresomes (Figs. 3D, E). Similarly, we found that Hsp70 was detectable in tNhtt-60Q aggresomes as expected but not in seipin inclusions (Fig. 3F).

To directly compare formation of seipin inclusions aggresome formation, we next co-transfected cells such that they express both mutant seipin and tNhtt-60Q. As shown in Fig. 3G, mutant seipin is not recruited to tNhtt-60Q-aggresomes and instead, forms independent inclusions. We conclude that formation of seipin inclusions occurs via a different mechanism than formation of tNhtt-60Q-aggresomes.

Transmembrane domains are critical for formation of seipin inclusions and induction of UPR by mutant seipin

To identify seipin sequences required for the formation of inclusion bodies, the subcellular distributions of deleted forms of seipin were
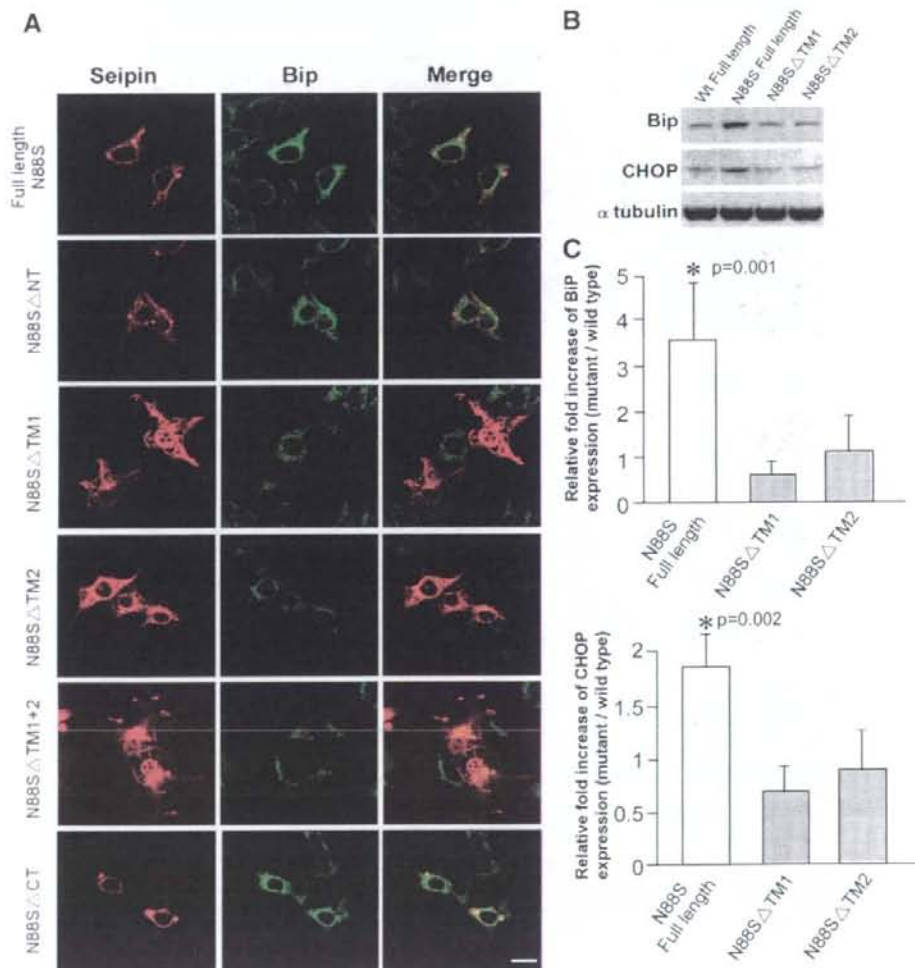

Fig. 4. A specific domain in a mutant form of seipin is responsible for the formation of inclusion bodies and activation of UPR. (A) Representative micrographs of HeLa cells following transfection with full-length seipin or deletion constructs that also carry the N88S mutation. The cells were then fixed and immunostained with anti-myc (9E10) to detect seipin and anti-GRP 78. Scale bar indicates 10 μm. (B) Immunoblot analysis of UPR molecules BiP and CHOP in transfected N2a cells. α-tubulin served as an internal loading control. (C) Quantitative analysis of BiP and CHOP protein induction. Immunoblots were scanned and analyzed by densitometry. The graph shows the fold increase in BiP and CHOP expression compared to that in the full-length wild-type. The values represent means±S.D. of six independent experiments. Asterisks (*) indicate a significant difference vs. full-length wild-type seipin (P<0.003).

examined by confocal microscopy. As shown in Fig. 4, NH2 or COOH-terminal deletions of seipin (ΔNT, ΔCT) that include the N88S single amino acid change result in inclusion formation. By contrast, no inclusions were detected in cells expressing a form of the N88S mutant seipin that lacks one or both transmembrane domains (ΔTm1, ΔTm2, ΔTm1+2, ΔTm1−2). Although the subcellular distribution of
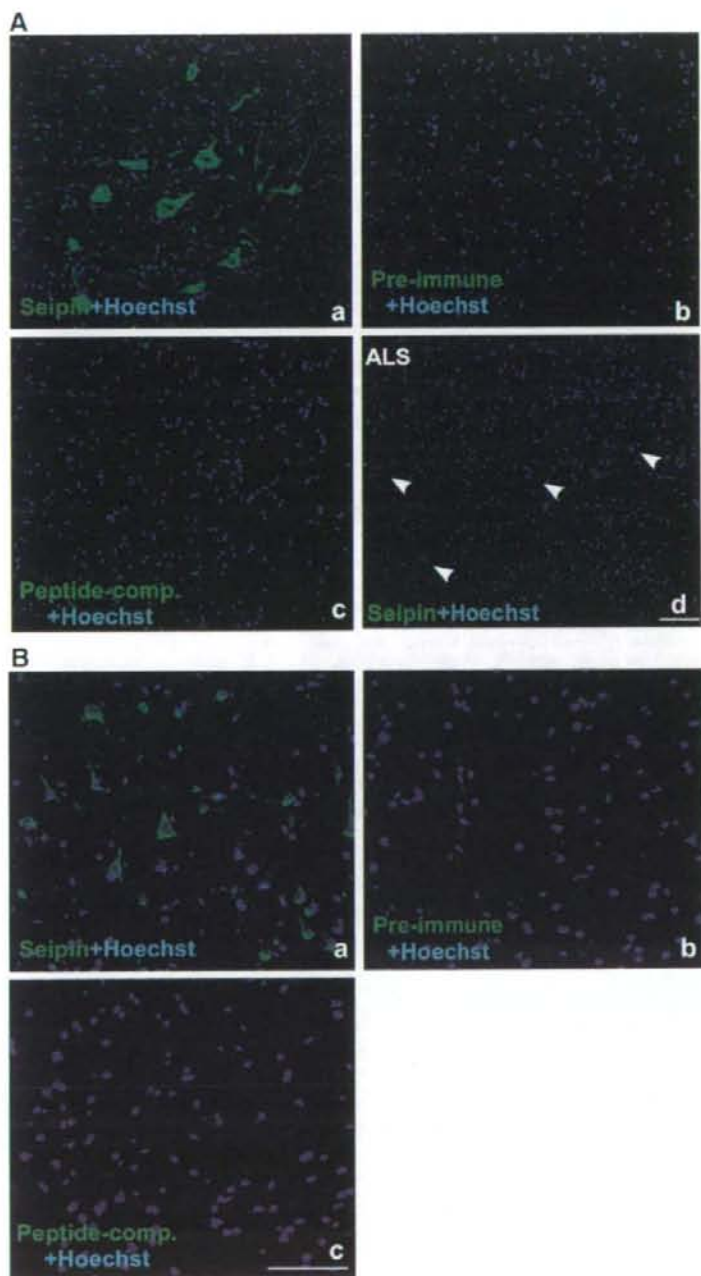

Fig. 5. Seipin expression in the human spinal cord and brain. (A) Human normal spinal cord samples were immunostained with (a) SCT14 antiserum, (b) preimmune serum, or (c) serum pre-absorbed by pre-incubation with excess C-terminal peptide of human seipin (ACGALRQRPTCSSS), followed by a general nuclear counter-stain (Hoechst). SCT14-stained motor neurons were observed in the anterior horns of normal spinal cords. Image (d) shows ALS-affected spinal cords stained with SCT14 antiserum. Arrowheads indicate degenerated motor neurons. Scale bar indicates 50 μm. (B) Human frontal lobe cortex immunostained with (a) SCT14 antiserum or (b) preimmune serum, and (c) serum pre-absorbed with peptide. Note that a strong seipin immunoreactive signal is detected in cortical neurons. Scale bar indicates 50 μm.

the ΔTm2 form of the N88S mutant protein is similar to wild-type, expression of this form does not result in the formation of inclusions, indicating that the second transmembrane domain is critical for inclusion formation.

The results of a previous study demonstrated that expression of N88S and S90L mutant seipin induces ER stress in N2a cells. We next assessed the levels of well-established UPR markers (namely, the ER chaperon BiP and the proapoptotic transcription factor CHOP) in N2a cells transfected with N88S mutant seipin forms that lack one or the other of the two transmembrane domains (ΔTm1, ΔTm2). As shown in Figs. 4B and C, both BiP and CHOP were up-regulated as compared to wild-type in cells expressing full-length mutant seipin (mean± standard deviation: CHOP, 1.89±0.29; BiP, 3.53±1.30), but the effect is not observed in cells that express N88S-ΔTm1 or ΔTm2 (for N88S-ΔTm1; CHOP, 0.70±0.26 and BiP, 0.53±0.39; for N88S-ΔTm2; CHOP, 0.87±0.25; BiP, 1.07±0.98), suggesting that both transmembrane domains are critical for activation of UPR.

Expression of seipin in specific tissues

The results of RNA blot analysis have shown that seipin mRNA is expressed at high levels in the brain and testis (Agarwal et al., 2002; Windpassinger et al., 2004). We previously demonstrated that immunoreactivity of a specific antiserum against seipin is detected in

motor neurons in the mouse spinal cord. In this study, we performed immunohistochemical analysis of seipin in various tissues, including in human brain tissue. To do this, we used SCT14, a polyclonal antiserum directed against the C-terminal peptide of human seipin (Ito and Suzuki, 2007a).

As shown in Figs. 5A and B, strong immunoreactivity of SCT14 antiserum was observed in motor neurons in the human spinal cord and cortical neurons in the frontal lobe, as expected from immunostaining of mouse spinal cords (Ito and Suzuki, 2007a). We also examined sections of tissue from a patient with the common motor neuron disease sporadic ALS. In that sample tissue, only faintly stained cells are detected in the anterior horn, consistent with degeneration of motor neurons (Fig. 5Ad).

In cryosections from mouse testes, seipin immunostaining is specifically observed in spermatids (Fig. 6). Interestingly, seipin is detected beginning around step 1–2 of spermatid development and subsequently increases in intensity, peaking at step 6–7 (Fig. 6B). Seipin is virtually undetectable in spermatozoa and it is undetectable in spermatogonia, spermatocytes, and Sertoli cells.

Bioinformatics search of data in the Human GeneAtlas from the Genomic Institute of the Novartis Research Foundation (http://symatlas.gnf.org/SymAtlas/) reveals that the pituitary gland shows strong expression of seipin. For this reason, we also checked regional localization of seipin in the mouse pituitary gland. As show in Fig. 7,
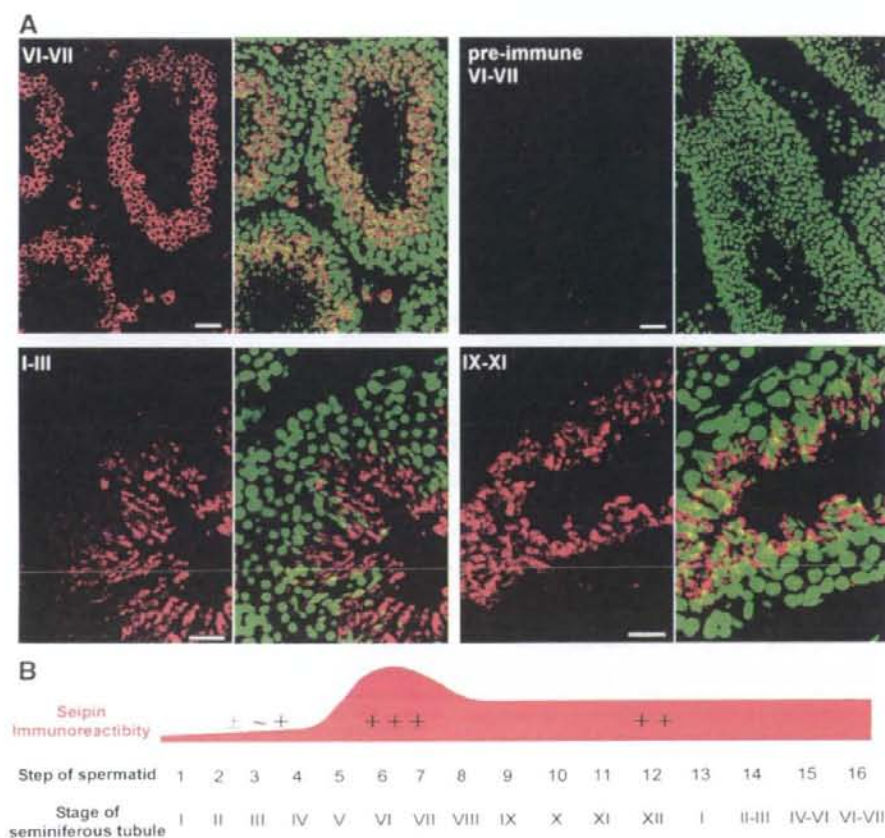

Fig. 6. Localization of seipin in the seminiferous tubules of adult mouse testes. (A) Frozen mouse testis sections were immunostained with SCT14 antiserum (red) and counterstained with SYTOX Green to visualize nuclear DNA (green). Images represent seminiferous tubules of stages VI–VII, I–III, IX–XI. Seipin immunoreactivity was specifically observed in spermatids and was not detected in spermatogonia, spermatocytes or Sertoli cells. (B) Seipin expression as it relates to steps in spermatid development. Seipin is detected at peak levels at step 6–7 of spermatid. Scale bar indicates 20 μm.
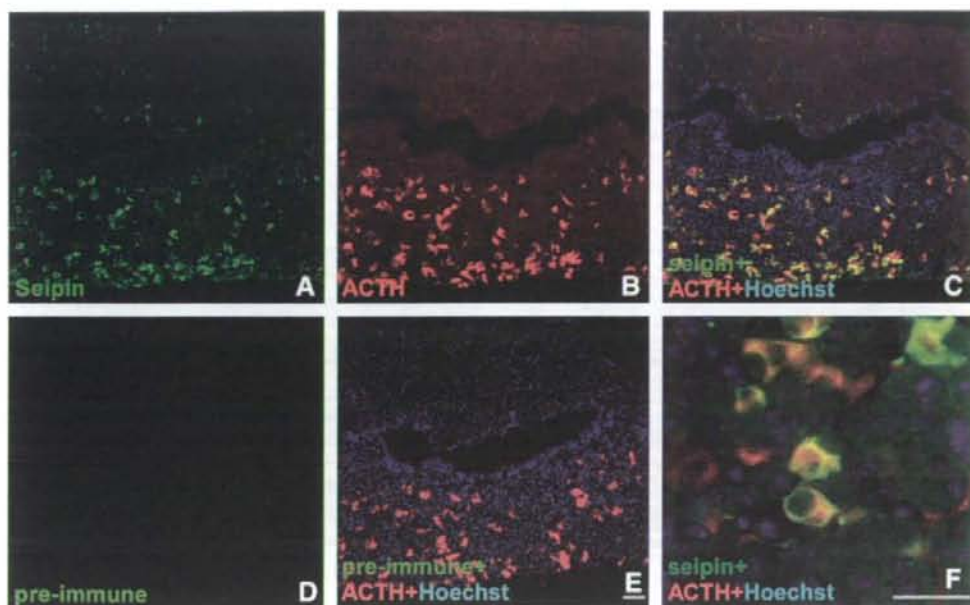
Fig. 7. Expression of seipin in the pituitary gland. The mouse pituitary gland was double-labeled with SCT14 (a, c, f) or preimmune serum (d, e) and an anti-ACTH antibody (b, c, e, f). Note in the high-magnification image (f) that seipin immunoreactivity is detected in ACTH-positive cells. Scale bar indicates 50 μm.

seipin immunoreactivity is detected in ACTH-positive cells from the anterior lobe of the pituitary gland.

Discussion

This study presents several interesting findings relevant to the localization and structure of human seipin and to the characteristics of seipin-containing inclusion bodies. We have demonstrated that wild-type seipin and a disease-associated mutant form of seipin are ER-resident transmembrane proteins. Moreover, seipin has a glycosylated loop that faces the ER lumen, and both protein termini face the cytosol (Fig. 1). These findings support the model of seipin membrane topology proposed by Lundin et al. (Lundin et al., 2006). Furthermore, we found that the first transmembrane domain in seipin is necessary for ER retention and that the second is critical for ubiquitination and formation of inclusions (Fig. 2). Because these regions have been highly evolutionarily conserved (Agarwal and Garg, 2004), it seems likely that these domains are essential for proper topology and modification of seipin in diverse organisms. Additionally, we detected no difference between wild-type and seipinopathy-related mutant proteins in fractionation or protease protection assays. Thus, our results suggest that the pathogenesis of seipinopathies cannot be attributed to an absence of seipin or gross mislocalization, as the mutant protein is clearly expressed and appears to have the same subcellular distribution as wild-type seipin.

We also characterized seipin inclusion bodies, which appear in cells expressing a mutant form of seipin. Over-expression of many pathogenic proteins, including mutant forms of huntingtin, α synuclein, parkin, and prion proteins can lead to accumulation of the mutant protein and formation of aggresomes (Garcia-Mata et al., 1999; Johnston et al., 1998; Junn et al., 2002; Kopito, 2000; Lee and Lee, 2002; Mishra et al., 2003; Muqit et al., 2004; Tanaka et al., 2004; Tran and Miller, 1999; Waelter et al., 2001). Kopito suggests that aggresomes form via the assembly of misfolded proteins at the MTOC in a microtubule-dependent manner (Kopito, 2000). Another characteristic feature of aggresomes is that intermediate filament proteins such as vimentin are redistributed

around the exterior of aggresomes, such as around aggregated tNhtt-60Q (see Fig. 3C) (Johnston et al., 1998; Kopito, 2000). Aggresomes are also enriched in molecular chaperons, including Hsc70 and Hsp40 (Garcia-Mata et al., 1999; Junn et al., 2002; Tanaka et al., 2004). In addition, most mutant proteins in aggresomes are reported to be poly-ubiquitinated and co-localize with chaperons. Indeed, several authors have suggested that the formation of aggresomes is a cellular response to the presence of misfolded proteins (Johnston et al., 1998; Kopito, 2000; Kopito and Ron, 2000).

In this work, neither ubiquitin nor Hsp70 was detected at significant levels in seipin inclusions, whereas seipin present in reticular patterns in the cell body does co-localize with ubiquitin immunoreactivity (Figs. 3D–F), consistent with detection of a high molecular weight seipin complexes by SDS-PAGE (Ito and Suzuki, 2007a). Ubiquitin is typically recruited to aggresomes; however, some aggresomes, such as those that form in the presence of the normally cytoplasmic proteins GFP250 and superoxide dismutase 1 do not show significant ubiquitination and are thought to be degraded in an ubiquitin-independent manner (Garcia-Mata et al., 1999; Johnston et al., 2000). It remains unclear if this variability reflects differences in specificity or affinity of molecular chaperons, in selectivity of deubiquitinating enzymes, or in variability of experimental conditions. Moreover, it is possible that non-ubiquitinated seipin evades ubiquitin-dependent degradation and that it is this pool of seipin in the cell that aggregates to form inclusions. Our results show that seipin-induced inclusion bodies have several properties that distinguish them from aggresomes, particularly in terms of the component proteins that make up the inclusion. Furthermore, unlike aggresomes, seipin inclusion bodies are not associated with the MTOC (Fig. 3B) and do not seem to affect the distribution of vimentin (Fig. 3C). This finding is strongly supported by the results of co-transfection of cells with mutant seipin and tNhtt-60Q, in which seipin inclusions and aggresomes do not co-localize (Fig. 3G), indicating that seipin inclusions form via a distinct pathway.

We also found that UPR is not activated in cells transfected with a mutant form of seipin lacking the first or second transmembrane domain. As described above, ER retention in disrupted by the ΔTm1

mutation (Fig. 2C) and the ΔTm2 form of seipin do not form the same high molecular weight complex or inclusions bodies observed for other forms (Figs. 2B and 4), suggesting that the ΔTm2 deletion does not lead to production of a misfolded protein. Therefore, it seems likely that misfolded mutant seipin lacking transmembrane domains does not accumulate in the ER and consequently, does not activate UPR.

Interestingly, the normal distribution of seipin in specific tissues appears to correlate with the disease state. Seipin is clearly expressed in motor neurons in the human spinal cord, consistent with pathologic phenotypes described in patients with seipinopathies, including a disturbance of lower motor neuron function (Fig. 5A). Moreover, seipin is localized in cortical neurons in the frontal lobe (Fig. 5B). Some subtypes of seipinopathies, such as SPG17, show spastic paraplegia, consistent with a disturbance of upper motor neuron function. Additionally, the presence of mutant seipin in frontal lobe could explain degeneration of upper motor neurons. These findings support an idea we proposed previously, that accumulation of unfolded mutant seipin in motor neurons causes neurodegeneration (Ito and Suzuki, 2007a).

We also detected seipin immunoreactivity in spermatids and in the anterior lobe of the pituitary gland (Figs. 6 and 7). CGL2 patients, which are homozygous for a null mutation in seipin, have defects the reproduction and endocrine systems, in particular abnormal secretion of anterior pituitary hormones (Agarwal and Garg, 2003, 2004; Fu et al., 2004; Mabry et al., 1973). Thus, seipin may have as yet unidentified functions during spermatogenesis and in the pituitary hypothalamic system. In contrast, human patients with seipinopathies are not known to have defects in endocrine function or fertility, suggesting that the mutations associated with seipinopathies (N88S and S90L) specifically affect motor neurons. Further study may help to uncover the tissue-dependent effects of these mutations, which we speculate could be the result of tissue-specific differences in protein folding and protein degradation.

Recently, two groups reported important evidence regarding the function of seipin (Fei et al., 2008; Szymanski et al., 2007). They demonstrated that yeast seipin is localized at junctions between the endoplasmic reticulum and a lipid droplet (the so-called lipid bodies or adiposomes) and that deletion of seipin results in irregular lipid droplets, indicating that yeast seipin is required for assembly or maintenance of lipid droplets. This finding implies that human seipin may also be associated with formation of lipid droplets and further, that a failure in that process is the primary cause of CGL2. However, adipose tissues dose not show substantial expression of seipin as measured by RNA blot analysis (Magre et al., 2001) and we did not detect significant immunoreactivity in adipose tissue (data not shown). Thus, it is possible that human seipin is a tissue-specific and multi-functional protein but further study is necessary to understand the functions of seipin.

Taken together, the data presented here demonstrate that the transmembrane domains of seipin are critical for subcellular localization, topology, formation of inclusions and activation of UPR by mutant forms of the protein. Moreover, seipin inclusions have unique characteristics and appear to be distinct from aggresomes. Moreover, we found that seipin is expressed in tissues other than motor neurons, suggesting roles in other biological processes, including endocrine function and spermatogenesis. However, it should be kept in mind that these suppositions are mainly based on studies of seipin overexpression in cultured cells. Subsequent studies are needed to test if what we found is also true of endogenous seipin protein *in vivo*. Unfortunately, very little is known about seipinopathies, as no pathological studies of affected patient tissues have been reported. In fact, to the best of our knowledge, no autopsy of a patient with seipinopathy has been reported, perhaps because seipinopathies are rare and are not fatal. Thus, a detailed examination using a transgenic mouse model seems important to verify the formation and characteristics of inclusions *in vivo*. Further study of the pathohistology of mutant forms of seipin should also be informative and together with

the results presented here, may lead to important new insights into motor neuron diseases, including other spastic paraplegia diseases and amyotrophic lateral sclerosis.

References

Agarwal, A.K., Garg, A., 2003. Congenital generalized lipodystrophy: significance of triglyceride biosynthetic pathways. Trends Endocrinol. Metab. 14, 214–221.
Agarwal, A.K., Garg, A., 2004. Seipin: a mysterious protein. Trends Mol. Med. 10, 440–444.
Agarwal, A.K., et al., 2002. AGPAT2 is mutated in congenital generalized lipodystrophy linked to chromosome 9q34. Nat. Genet. 31, 21–23.
Arrasate, M., et al., 2004. Inclusion body formation reduces levels of mutant huntingtin and the risk of neuronal death. Nature 431, 805–810.
Auer-Grumbach, M., et al., 2005. Phenotypes of the N88S Berardinelli-Seip congenital lipodystrophy 2 mutation. Ann. Neurol. 57, 415–424.
DiFiglia, M., et al., 1997. Aggregation of huntingtin in neuronal intranuclear inclusions and dystrophic neurites in brain. Science 277, 1990–1993.
Fei, W., et al., 2008. Fld1p, a functional homologue of human seipin, regulates the size of lipid droplets in yeast. J. Cell Biol. 180, 473–482.
Fu, M., et al., 2004. Mutations in Gng3lg and AGPAT2 in Berardinelli-Seip congenital lipodystrophy and Brunzell syndrome: phenotype variability suggests important modifier effects. J. Clin. Endocrinol. Metab. 89, 2916–2922.
Garcia-Mata, R., et al., 1999. Characterization and dynamics of aggresome formation by a cytosolic GFP-chimera. J. Cell Biol. 146, 1239–1254.
Hatakeyama, S., et al., 2001. U box proteins as a new family of ubiquitin-protein ligases. J. Biol. Chem. 276, 33111–33120.
Iida, H., et al., 2006. Spetex-1: a new component in the middle piece of flagellum in rodent spermatozoa. Mol. Reprod. Dev. 73, 342–349.
Irobi, J., et al., 2004. The phenotype of motor neuropathies associated with BSCL2 mutations is broader than Silver syndrome and distal HMN type V. Brain 127, 2124–2130.
Ito, D., et al., 1998. Microglia-specific localisation of a novel calcium binding protein, Iba1. Brain Res. Mol. Brain Res. 57, 1–9.
Ito, D., Suzuki, N. 2007a. Molecular pathogenesis of seipin/BSCL2-related motor neuron diseases. Ann. Neurol. 61, 237–250.
Ito, D., Suzuki, N., 2007b. [Seipin/BSCL2-related motor neuron disease, seipinopathy is a novel conformational disease associated with endoplasmic reticulum stress]. Rinsho Shinkeigaku 47, 329–335.
Ito, D., et al., 1999. Uncoupling of cerebral blood flow and glucose utilization in the regenerating facial nucleus after axotomy. Neurosci. Res. 35, 207–215.
Ito, D., et al., 2001a. Enhanced expression of Iba1, ionized calcium-binding adapter molecule 1, after transient focal cerebral ischemia in rat brain. Stroke 32, 1208–1215.
Ito, D., et al., 2001b. Up-regulation of the Ire1-mediated signaling molecule, Bip, in ischemic rat brain. NeuroReport 12, 4023–4028.
Johnston, J.A., et al., 1998. Aggresomes: a cellular response to misfolded proteins. J. Cell Biol. 143, 1883–1898.
Johnston, J.A., et al., 2000. Formation of high molecular weight complexes of mutant Cu, Zn-superoxide dismutase in a mouse model for familial amyotrophic lateral sclerosis. Proc. Natl. Acad. Sci. U. S. A. 97, 12571–12576.
Junn, E., et al., 2002. Parkin accumulation in aggresomes due to proteasome impairment. J. Biol. Chem. 277, 47870–47877.
Kalchman, M.A., et al., 1996. Huntingtin is ubiquitinated and interacts with a specific ubiquitin-conjugating enzyme. J. Biol. Chem. 271, 19385–19394.
Klement, I.A., et al., 1998. Ataxin-1 nuclear localization and aggregation: role in polyglutamine-induced disease in SCA1 transgenic mice. Cell 95, 41–53.
Kopito, R.R., 2000. Aggresomes, inclusion bodies and protein aggregation. Trends Cell Biol. 10, 524–530.
Kopito, R.R., Ron, D., 2000. Conformational disease. Nat. Cell Biol. 2, E207–E209.
Lee, H.J., Lee, S.J., 2002. Characterization of cytoplasmic alpha-synuclein aggregates. Fibril formation is tightly linked to the inclusion-forming process in cells. J. Biol. Chem. 277, 48976–48983.
Lundin, C., et al., 2006. Membrane topology of the human seipin protein. FEBS Lett. 580, 2281–2284.
Mabry, C.C., et al., 1973. Pituitary-hypothalamic dysfunction in generalized lipodystrophy. J. Pediatr. 82, 625–633.

Magre, J., et al., 2001. Identification of the gene altered in Berardinelli-Seip congenital lipodystrophy on chromosome 11q13. Nat. Genet. 28, 365–370.

Mishra, R.S., et al., 2003. Aggresome formation by mutant prion proteins: the unfolding role of proteasomes in familial prion disorders. J. Alzheimer's Dis. 5, 15–23.

Muqit, M.M., et al., 2004. Parkin is recruited into aggresomes in a stress-specific manner: over-expression of parkin reduces aggresome formation but can be dissociated from parkin's effect on neuronal survival. Hum. Mol. Genet. 13, 117–135.

Orr, H.T., 2004. Neurodegenerative disease: neuron protection agency. Nature 431, 747–748.

Saudou, F., et al., 1998. Huntingtin acts in the nucleus to induce apoptosis but death does not correlate with the formation of intranuclear inclusions. Cell 95, 55–66.

Sieradzan, K.A., et al., 1999. Huntington's disease intranuclear inclusions contain truncated, ubiquitinated huntingtin protein. Exp. Neurol. 156, 92–99.

Sisodia, S.S., 1998. Nuclear inclusions in glutamine repeat disorders: are they pernicious, coincidental, or beneficial? Cell 95, 1–4.

Szymanski, K.M., et al., 2007. The lipodystrophy protein seipin is found at endoplasmic reticulum lipid droplet junctions and is important for droplet morphology. Proc. Natl. Acad. Sci. U. S. A.

Tanaka, M., et al., 2004. Aggresomes formed by alpha-synuclein and synphilin-1 are cytoprotective. J. Biol. Chem. 279, 4625–4631.

Taylor, J.P., et al., 2003. Aggresomes protect cells by enhancing the degradation of toxic polyglutamine-containing protein. Hum. Mol. Genet. 12, 749–757.

Tran, P.B., Miller, R.J., 1999. Aggregates in neurodegenerative disease: crowds and power? Trends Neurosci. 22, 194–197.

Wada, I., et al., 1994. Chaperone function of calnexin for the folding intermediate of gp80, the major secretory protein in MDCK cells. Regulation by redox state and ATP. J. Biol. Chem. 269, 7464–7472.

Waelter, S., et al., 2001. Accumulation of mutant huntingtin fragments in aggresome-like inclusion bodies as a result of insufficient protein degradation. Mol. Biol. Cell 12, 1393–1407.

Wang, G.H., et al., 1999. Caspase activation during apoptotic cell death induced by expanded polyglutamine in N2a cells. NeuroReport 10, 2435–2438.

Windpassinger, C., et al., 2004. Heterozygous missense mutations in BSCL2 are associated with distal hereditary motor neuropathy and Silver syndrome. Nat. Genet. 36, 271–276.

Contents lists available at ScienceDirect

Journal of the Neurological Sciences

journal homepage: www.elsevier.com/locate/jns

Cardiac parasympathetic dysfunction concurrent with cardiac sympathetic denervation in Parkinson's disease

Mamoru Shibata [a,b,*], Yoko Morita [a], Toshihiko Shimizu [b], Kazushi Takahashi [b], Norihiro Suzuki [b]

[a] Department of Neurology, National Hospital Organization Tokyo Medical Center, 2-5-1 Higashigaoka, Meguro-ku, Tokyo 152-8902, Japan
[b] Department of Neurology, School of Medicine, Keio University, 35 Shinanomachi, Shinjuku-ku, Tokyo 160-8582, Japan

ARTICLE INFO

ABSTRACT

We aimed to characterize the relationship between cardiac sympathetic and parasympathetic dysfunction employing cardiac ^{123}I-meta-iodobenzylguanidine (MIBG) uptake and other autonomic function parameters in Parkinson's disease (PD). 79 PD patients were studied. We performed ^{123}I-MIBG myocardial scintigraphy to assess the extent of cardiac sympathetic denervation. Electrocardiogram readings at rest and postural change in blood pressure were also examined. Coefficient variation of RR intervals (CVR-R) was used as an index for cardiac parasympathetic activity. Cardiac ^{123}I-MIBG uptake did not vary significantly among the Hoehn–Yahr (H–Y) stages. There was a significant correlation between cardiac ^{123}I-MIBG uptake and CVR-R (early, $r=0.457$, $p<0.001$; late, $r=0.442$, $p<0.001$). While the correlation was present among the patients who had had the disease less than two years (early, $r=0.558$, $p<0.001$; late, $r=0.530$, $p<0.001$), the patients with the disease duration longer than two years did not have such a significant correlation. Age, disease duration, corrected QT interval, or postural blood pressure change did not correlate with cardiac ^{123}I-MIBG uptake. Orthostatic hypotension was observed in 13 out of 72 subjects, and reduced CVR-R was a major determinant for the development of orthostatic hypotension. We conclude that cardiac parasympathetic dysfunction occurs concurrent with sympathetic denervation as revealed by ^{123}I-MIBG myocardial scintigraphy in PD and contributes to the development of orthostatic hypotension.

© 2008 Elsevier B.V. All rights reserved.

1. Introduction

Recent evidence shows that Parkinson's disease (PD) is a neurodegenerative disease that manifests a constellation of neurological symptoms beyond classic Parkinsonian features, such as resting tremor and rigidity, and forms a continuum with dementia with Lewy bodies (DLB) characterized by limbic and neocortical degeneration responsible for cognitive impairment [1]. Braak et al. [2] clarified that pathological processes in PD begin in the anterior olfactory nucleus and medulla, the latter of which harbors the dorsal motor nucleus of the vagal nerve, one of major autonomic centers. Accordingly, hyposmia and autonomic dysfunction, particularly constipation, are now appreciated as early clinical manifestations relevant to PD. Recognition of these symptoms will become more important with attempts to institute preventive therapy against this disabling disease.

The peripheral autonomic system is also affected in PD. Pathological studies have demonstrated the presence of Lewy bodies in myenteric and submucosal plexuses [3–5]. As for the cardiac autonomic system, many nuclear radiological studies using ^{123}I-meta-iodobenzylguanidine

(MIBG) or 6-[^{18}F]fluorodopamine have reported cardiac sympathetic denervation in PD patients, and the degeneration of postganglionic sympathetic fibers was confirmed by postmortem pathological examinations [6,7]. However, the absence of obvious cardiovascular symptoms, like orthostatic hypotension, in many of cases displaying reduced cardiac ^{123}I-MIBG uptake is an enigma [8,9]. This implies a need for a comprehensive understanding of cardiovascular autonomic status including cardiac parasympathetic and peripheral vasomotor activity and cardiac sympathetic function. Despite the presence of several hemodynamic studies showing the involvement of cardiac parasympathetic system in PD [9–13], its incidence and temporal profile relative to cardiac sympathetic denervation remain elusive.

Here, we demonstrate that cardiac parasympathetic dysfunction occurs with sympathetic denervation in PD by examining heart rate variability at rest and cardiac ^{123}I-MIBG uptake. Concurrent development of parasympathetic and sympathetic dysfunction is obvious in the early stages of PD.

2. Methods

2.1. Subjects

79 PD patients (39 men and 40 women) who visited our outpatient clinic were studied. All patients fulfilled United Kingdom Parkinson's

* Corresponding author. Department of Neurology, School of Medicine, Keio University, 35 Shinanomachi, Shinjuku-ku, Tokyo 160-8582, Japan. Tel.: +81 3 5363 3788; fax: +81 3 3353 1272.
E-mail address: mshibata@sc.itc.keio.ac.jp (M. Shibata).

Table 1

Comparisons of demographic and autonomic function parameters other than H/M ratio of ^{123}I-meta-iodobenzylguanidine (MIBG) among the Hoehn–Yahr stages

Hoehn–Yahr stage	I	II	III	IV	V	p
N	20	29	23	5	2	
Age, y	71.0±5.2	72.5±6.9	76.4±5.5	75.2±5.5	74.0±4.2	NS
Gender (M:F)	8:12	15:14	10:13	3:2	0:2	NS
Disease duration, y	1.4±1.1	3.5±4.0	4.2±4.6	6.0±6.1	10.5±6.4	NS
						p=0.017[a]
Age of onset, y	69.4±5.4	69.0±8.7	72.3±8.0	69.2±10.7	63.5±10.6	NS
WR (%)	32.7±7.1	33.0±6.3	33.2±6.1	29.9±3.5	26.2±5.0	NS
CVR-R (%)	2.50±1.26	2.11±0.89	2.26±1.23	1.40±0.40	0.81±0.13	NS
QTc (ms)	412±15	408±16	411±15	425±21	433±1	NS
ΔSBPp (mm Hg)	−4.2±15.3	−6.5±17.6	−4.9±16.5	−11.0±15.7	−5.5±16.2	NS

Data are mean±SD. NS=not significant.
[a] Post-hoc comparison I vs. V.

Disease Society Brain Bank Clinical Diagnosis Criteria [14]. Other Parkinsonian disorders such as vascular parkinsonism, multiple system atrophy, and progressive supranuclear palsy were excluded from clinical features and MRI findings. None of the subjects exhibited marked dementia or visual hallucination. Those who had ischemic heart disease, diabetes mellitus, or were undergoing treatment with selegiline hydrochloride (L-deprenyl) or tricyclic antidepressants were not included in consideration of the potential effects of these factors on cardiac ^{123}I-MIBG uptake. We employed the Hoehn–Yahr (H–Y) stage to assess the disease severity. 44 of the 79 subjects were on medication for PD at the time of investigation. We evaluated motor symptoms during the "off" period when we examined medicated patients. The mean age±SD was 73.4±6.2 years, and the mean disease duration±SD, 3.5±4.1 years.

Informed consent was obtained from every patient prior to enrollment. This study was approved by the institutional review board for clinical research of the National Hospital Organization Tokyo Medical Center.

2.2. ^{123}I-MIBG myocardial scintigraphy

The patients were asked not to have breakfast on the day of examination. Each subject was relaxed in the supine position for 20 min and was intravenously injected with 111 MBq of ^{123}I-MIBG (Daiichi Radioisotope Laboratories Co., Tokyo, Japan) around 10:00 AM. A thoracic planar image was acquired in a static fashion for 5 min

using a dual-headed rotating scintillation camera (HITACHI gamma-view-i RPC-DC) equipped with low-energy, high-resolution parallel-hole collimators after 15 min (early phase) and 3 h (late phase) following the administration of ^{123}I-MIBG. The acquisition matrix was 256×256. Energy discrimination was centered on 159 keV with a 10% window. In each case, an oval region of interest (ROI) was set on the left ventricular part of the heart with a rectangular reference ROI placed on the upper mediastinum of the anterior ^{123}I-MIBG planar image. Average counts per pixel were made in these ROIs. The heart-to-mediastinum (H/M) ratios for the early and late images were calculated to evaluate the integrity of cardiac sympathetic nerve fiber densities. The washout ratio (WR) was defined as 100×(Ec−Lc)/Ec % (Ec: the early cardiac count density, Lc: the decay-corrected late cardiac count density).

2.3. Electrocardiogram analysis and postural change in systolic blood pressure

After a bed rest for 5 min, an electrocardiogram (EKG) recording in the supine position with normal breathing was carried out for 5 min using ECG-1550 (Nihon Kohden). For analysis of coefficient variation of RR intervals (CVR-R), successive 200 RR intervals were sampled during the recording period. CVR-R was automatically calculated as a percentage of the standard deviation of the RR intervals divided by their mean. CVR-R measured at rest under normal breathing is an established index for parasympathetic activity [15,16]. QTc was computed according to Bazett's formula; $QTc=QT/(RR)^{1/2}$. Blood pressure was measured in the supine position. Subsequently, blood pressure in the upright position was recorded after 60-second-long orthostasis. Postural change in systolic blood pressure (ΔSBPp) was also calculated.

2.4. Statistical analysis

The data were analyzed using the SPSS software, version 15.0 Family (SPSS Inc., Chicago, IL.). Inter-group differences were evaluated using one-way analysis of variance (ANOVA) combined with Tukey's post-hoc test or unpaired t-test. χ^2 calculations were used for frequency data. Correlations for the H/M ratio of MIBG uptake, CVR-R, QTc, heart rate (HR), and postural change in systolic blood pressure were assessed using Pearson's correlation coefficient. Multiple regression analyses were performed on the correlation of H/M ratio of MIBG uptake with other parameters. p value <0.01 was considered statistically significant.

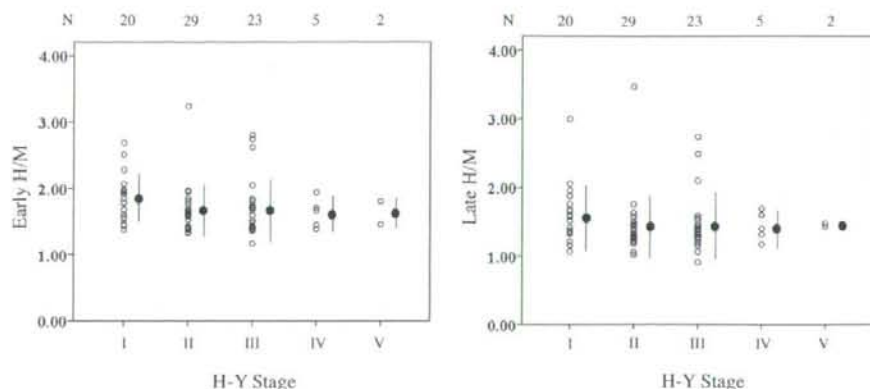**Fig. 1.** Comparisons of H/M ratio of ^{123}I-meta-iodobenzylguanidine (MIBG) uptake among the Hoehn–Yahr (H–Y) stages. The dot and bar data represent mean±SD. The data were analyzed using one-way analysis of variance and Tukey's post-hoc test.

81

3. Results

3.1. Comparisons of cardiac ^{123}I-MIBG uptake and autonomic function-related parameters among the H–Y stages

Of the 79 PD patients, we rated 20 patients as H–Y stage I, 29 as H–Y stage II, 23 as stage III, 5 as H–Y stage IV, and 2 as H–Y stage V, on the basis of their clinical manifestations. Using EKGs, we detected atrial fibrillation (Af) in two subjects, premature atrial contractions (PACs) in one, premature ventricular contractions (PVCs) in two, and both Af and PVC in one patient. Such cases were excluded from the analysis of CVR-R and QTc. Additionally, 5 subjects had right bundle branch block (RBBB), and they were eliminated from the QTc analysis. Blood pressure data were available in 72 cases. Orthostatic hypotension (ΔSBPp$\leq$−20 mm Hg) was observed in 13 cases (three in H–Y stage I, three in H–Y stage II, four in H–Y stage III, two in H–Y stage IV, and one in H–Y stage V). As shown in Table 1, among the H–Y stages, we found no statistically significant differences in age, disease duration, or sex ratios. There was a trend for a disease stage-dependent reduction in the H/M ratio in the early image (early H/M), and late image (late H/M) of ^{123}I-MIBG uptake (Fig. 1), but statistical significance was not reached because of considerable variations. We did not find any statistically significant difference in WR, CVR-R, QTc, or ΔSBPp (Table 1). These findings suggest that cardiovascular autonomic dysfunction in PD is likely to develop independent of motor impairment, although our data contain only two patients with H–Y stage V.

3.2. Correlations of cardiac ^{123}I-MIBG uptake with autonomic function parameters

In a univariate analysis, there was a significant correlation between H/M ratio and CVR-R (early, $r=0.457$, $p<0.001$; late, $r=0.442$, $p<0.001$; Fig. 2A). We confirmed that there was no significant correlation between CVR-R and age in our subjects ($r=0.086$, $p=0.469$), which excluded the possibility that aging was a significant confounding factor in our study. Subsequently, we performed a sub-analysis using the data obtained only from the PD patients with a duration of illness less than two years. Interestingly, significant correlations between H/M ratio and CVR-R were demonstrated in these patients (early, $r=0.558$, $p<0.001$; late, $r=0.530$, $p<0.001$; Fig. 2B), while such correlations were not detected in subjects having a disease duration beyond two years (data not shown).

On the other hand, WR did not correlate with CVR-R ($r=-0.108$, $p=0.365$). QTc did not correlate significantly with the H/M ratio (early, $r=0.001$, $p=0.995$; late, $r=0.065$, $p=0.597$).

We also looked at the correlation between HR and either of H/M ratio or CVR-R. There was no correlation between HR and H/M ratio (HR vs. early H/M, $r=0.063$, $p=0.583$; HR vs. late H/M, $r=0.058$, $p=0.613$). Meanwhile, there was a weak correlation between HR and CVR-R ($r=-0.227$, $p=0.053$), although the correlation did not reach statistical significance (Fig. 3).

Obvious orthostatic hypotension (ΔSBPp$\leq$−20 mm Hg) was observed in 13 out of 72 cases in which blood pressure data were available. One reason for such a low frequency might be that we did
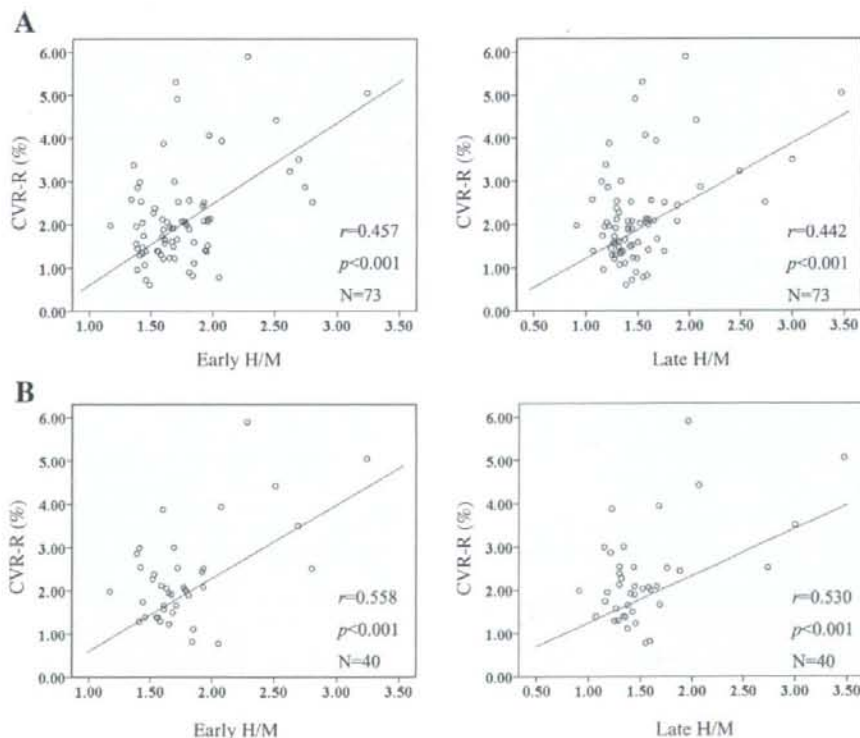
Fig. 2. Correlations between H/M ratio of ^{123}I-meta-iodobenzylguanidine (MIBG) uptake and coefficient variation of RR intervals (CVR-R). (A) Significant correlations were found between H/M ratio of ^{123}I-MIBG at both early and late stages and CVR-R (early, $r=0.457$, $p<0.001$; late, $r=0.442$, $p<0.001$). (B) Using the data obtained only from the subjects with a duration of illness less than two years, the correlations H/M ratio of ^{123}I-MIBG at both early and late stages and CVR-R were significant (early, $r=0.558$, $p<0.001$; late, $r=0.530$, $p<0.001$).
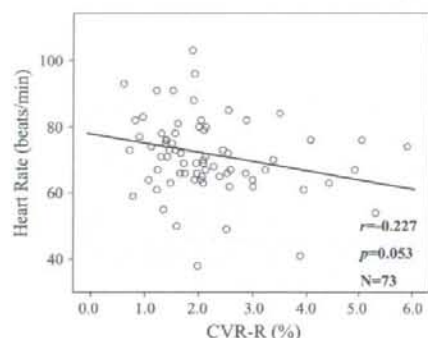
Fig. 3. Correlations between heart rate (HR) and coefficient variation of RR intervals (CVR-R). There was a weak correlation between HR and CVR-R, although the correlation did not reach statistical significance ($r = -0.227$, $p = 0.053$).

Table 3
Multiple regression analysis of correlation of cardiac ^{123}I-meta-iodobenzylguanidine (MIBG) uptake with demographic data and other autonomic function parameters

	Parameter estimate	SD	p
a. Early H/M			
Age	0.010	0.007	0.175
Disease duration	−0.012	0.010	0.271
CVR-R	0.118	0.040	0.004*
QTc	−0.002	0.003	0.494
ΔSBPp	0.004	0.003	0.113
b. Late H/M			
Age	0.010	0.008	0.250
Disease duration	−0.013	0.012	0.281
CVR-R	0.139	0.045	0.003*
QTc	0.001	0.003	0.871
ΔSBPp	0.007	0.003	0.036

*$p < 0.01$.

not adopt a head-up tilt technique [17]. However, our method where the subjects rose on their own appeared more relevant to their natural setting. We compared the demographic and autonomic function parameters between subjects with and without orthostatic hypotension. As shown in Table 2, among those factors, the difference in CVR-R was most prominent. We also performed multiple regression analysis concerning the correlation of cardiac ^{123}I-MIBG uptake and other parameters. Consistent with the univariate analysis, CVR-R exhibited a statistically significant correlation with both early and late H/M ratio (early, $p = 0.004$; late, $p = 0.003$). Nevertheless, age, disease duration, ΔSBPp, and QTc failed to show any significant correlation (Table 3).

4. Discussion

The present study demonstrates a significant positive correlation between the H/M ratio in the ^{123}I-MIBG myocardial scintigraphy and the CVR-R in patients with PD. Furthermore, our sub-analysis indicates that such a correlation can be attributed to the data obtained from the patients with a disease duration of less than two years. Our findings suggest that cardiac parasympathetic dysfunction occurs in parallel with cardiac sympathetic denervation in early PD patients. Plus, as the severity of cardiac autonomic parameter alterations was not proportional to the degree of motor impairment, the development of cardiac autonomic dysfunction is likely to be independent of the dopaminergic neurodegeneration responsible for motor symptoms. Our data also suggest that cardiac parasympathetic dysfunction plays a major role in the emergence of orthostatic hypotension in PD.

Recently, the importance of non-motor symptoms associated with PD, like hyposmia and autonomic dysfunction, has been emphasized.

Table 2
Comparisons of demographic data, H/M ratio of cardiac ^{123}I-meta-iodobenzylguanidine (MIBG) uptake, and other autonomic function parameters between patients with and without orthostatic hypotension (OH)

	Without OH ($n = 59$)	With OH ($n = 13$)	p
Age, y	72.9±6.4	74.0±5.0	0.480
Gender (M:F)	26:33	7:6	0.525
Disease duration, y	3.3±3.7	5.0±6.3	0.356
Age of onset, y	69.4±7.7	68.9±8.9	0.850
Early H/M ratio	1.77±0.39	1.64±0.17	0.062
Late H/M ratio	1.51±0.44	1.41±0.21	0.197
WR (%)	33.0±6.7	30.7±4.8	0.137
CVR-R (%)	2.30±1.20	1.65±0.50	0.004*
QTc (ms)	410±15	419±18	0.124

*$p < 0.01$.
Data are mean±SD.

These symptoms can be clinical manifestations attributable to early pathological processes in PD [2,18]. As for cardiac autonomic abnormalities, sympathetic denervation has been demonstrated by numerous studies employing either ^{123}I-MIBG myocardial scintigraphy or 6-[^{18}F] fluorodopamine cardiac PET [8,9,11–13,19,20]. Nevertheless, little information is available as to how the involvement of cardiac parasympathetic system develops in PD. Goldstein et al. [12] demonstrated that PD patients with orthostatic hypotension had a parasympathetic dysfunction, as evidenced by a reduced reflexive cardiovagal gain during the Valsalva maneuver. Moreover, Kallio et al. [21] demonstrated an abnormal cardiac parasympathetic activity in their 50 untreated PD patients by examining the high frequency component of RR intervals (RR-HF). Their results are in agreement with our finding that cardiac parasympathetic activity begins to decline with cardiac sympathetic denervation even in early PD patients. A recent report studying 44 untreated PD patients shows that RR-HF decreases with increasing disease severity, thus suggesting that cardiac parasympathetic dysfunction was a late event in PD [9]. There was no correlation between the RR-HF and the severity of cardiac sympathetic denervation despite ^{123}I-MIBG myocardial scintigraphy in their study. In another study, a weak correlation was found between heart rate variability and the latency of sympathetic skin response, the latter of which is a marker for sympathetic sudomotor activity [22]. Although it is accepted that there is cardiac parasympathetic dysfunction in PD, there seems to be a controversy as to the temporal profile of its development in relation to sympathetic abnormalities.

The heart rate variability at rest under normal breathing has been established as a reliable index of cardiac parasympathetic activity [15,16]. We measured the heart rate variability of 200 consecutive heartbeats, which took only a few minutes. This approach has several strengths. First, it does not require any strenuous act, such as the Valsalva maneuver, which can be unfeasible for PD patients with overt hypokinesia. A brief EKG recording in a supine position is suitable for PD patients, who often have motor impairment. Second, the heart rate variability at rest is almost free of the baroreflex function exerted by the glossopharyngeal afferent fibers from the carotid sinus and aortic arch, while that obtained during the Valsalva maneuver is susceptible to modulation by the vagal baroreflex. Our results raise the possibility that the abnormality lies in the vagal efferent system. Although some authors have detected abnormal changes in the heart rate variability indicative of parasympathetic dysfunctions during the Valsalva maneuver in PD, it was difficult to determine the site of abnormality in its complicated reflex arc [9,12]. Furthermore, destruction of nigrostriatal dopaminergic system *per se* has been demonstrated to affect baroreflex sensitivity in rats [23]. Despite the difference in species, this result suggests caution in interpreting the results from the Valsalva maneuver in PD. Third, our short-term EKG recording is less susceptible to the effect of arrhythmias. A recent study using a

83

45-minute-long EKG recording has disclosed a higher incidence of extrasystoles in 40 PD patients as compared to 80 normal subjects (55% vs 16.25%) [24]. Thus, a shorter recording should avoid the effect of arrhythmias, which render the accurate measurement of heart rate variability impossible. Lastly, as the CVR-R can be calculated very quickly, and does not entail any complicated analysis, it can provide immediate information on cardiac parasympathetic function. For these reasons, our method for measuring the CVR-R is an excellent means to assess cardiac parasympathetic activity of PD patients.

The parasympathetic abnormalities underlying the decreased heart rate variability in PD are unknown. From a physiological viewpoint, it can reflect a loss of function or a hypertonic state of the cardiac parasympathetic system. However, it is impossible to determine which of these is responsible from our findings alone. It was shown that the decrement of RR intervals in response to a decrease in blood pressure during the early second phase of the Valsalva maneuver was compromised, whereas the reflex bradycardia in the fourth phase was preserved in their de novo PD patients [9]. This favors the hypertonic state hypothesis, because the finding can be well explained by the inability of parasympathetic tone to diminish with declining blood pressure.

Concerning the underlying pathological changes, Benarroch et al. [25,26] showed that the ventrolateral nucleus ambiguus, a major locus of cardiac preganglionic vagal neurons [27,28], is spared in PD. Meanwhile, the dorsal motor nucleus of the vagal nerve provides a minor preganglionic parasympathetic projection to the cardiac ganglia, and cell loss and aberrant α-synuclein depositions identified as Lewy bodies and Lewy neurites in the brainstem nucleus are prominent in PD [2,26]. Consistent with the MIBG myocardial scintigraphy findings, the cardiac postganglionic sympathetic fiber degeneration has been verified by several pathological studies [6,7].

In contrast, information about the involvement of cardiac postganglionic vagal neurons in PD remains scanty [29,30]. Iwanaga et al. [29] noted the presence of Lewy bodies and Lewy neurites in the cardiac plexus. Intriguingly, those inclusions resided in both tyrosine hydroxylase-positive and -negative nerve processes, which suggested that PD affects parasympathetic fibers as well as sympathetic nerves in the heart. As incidental Lewy body disease cases were included in their study, there is the likelihood that the involvement of cardiac postganglionic parasympathetic fibers occurs even in the early stage of PD.

The paucity of cardiovascular symptoms, such as orthostatic hypotension, in PD patients with cardiac sympathetic denervation identifiable with ^{123}I-MIBG myocardial scintigraphy seems paradoxical, and therefore obscures the significance of the cardiac sympathetic denervation. Haensch et al. [31] also reported that reduced ^{123}I-MIBG myocardial uptake occurred irrespective of the presence of orthostatic hypotension. Our study suggests that the advancement of cardiac parasympathetic dysfunction in addition to sympathetic denervation may be a requirement for the development of orthostatic hypotension. Additionally, our data imply that impaired cardiac parasympathetic activity contributes more to determine HR than cardiac sympathetic denervation, although the impact of CVR-R change on HR is relatively small (Fig. 3). This is likely to explain why most of the PD patients with a low CVR-R value did not exhibit tachycardia at rest. Moreover, the possibility remains that concurrent cardiac sympathetic denervation may offset the effect of parasympathetic dysfunction.

In summary, this study provides important evidence for cardiac parasympathetic dysfunction in parallel to cardiac sympathetic denervation in early PD. Thus, our findings expand the spectrum of non-motor aspects of PD and highlight the character of PD as a multisystemic disorder even in its early stage.

Acknowledgments

References

[1] MacKeith I, Galasko D, Kosaka K, Perry EK, Dickson DW, Hansen LS, et al. Consensus guidelines for the clinical and pathologic diagnosis of dementia with Lewy bodies (DLB): report of the consortium on DLB international workshop. Neurology 1996;47:1113–24.

[2] Braak H, Del Tredici K, Rüb U, de Ros RAI, Jansen Steur ENH, Braak E. Staging of brain pathology related to sporadic Parkinson's disease. Neurobiol Aging 2003;24:197–211.

[3] Kupsky WJ, Grimes MM, Sweeting J, Bertsch R, Cote LJ. Parkinson's disease and megacolon: concentric hyaline inclusions (Lewy bodies) in enteric ganglion cells. Neurology 1987;37:1253–5.

[4] Wakabayashi K, Takahashi H, Takeda S, Ohama E, Ikura F. Parkinson's disease: the presence of Lewy bodies in Auerbach's and Meissner's plexuses. Acta Neuropathol 1988;76:217–21.

[5] Wakabayashi K, Takahashi H. Neuropathology of autonomic nervous system in Parkinson's disease. Eur Neurol 1997;38(suppl 2):2–7.

[6] Amino T, Orimo S, Itoh Y, Takahashi A, Uchihara T, Mizusawa H. Profound cardiac sympathetic denervation occurs in Parkinson's disease. Brain Pathol 2005;15:29–34.

[7] Orimo S, Takahashi A, Uchihara T, Mori F, Kakita A, Wakabayashi K, et al. Degeneration of cardiac sympathetic nerve begins in the early disease process of Parkinson's disease. Brain Pathol 2007;17:24–30.

[8] Courbon F, Brefel-Courbon C, Thalamas C, Alibelli MJ, Berry I, Montastruc JL, et al. Cardiac MIBG scintigraphy is a sensitive tool for detecting cardiac sympathetic denervation in Parkinson's disease. Mov Disord 2003:890–7.

[9] Oka H, Mochio S, Onouchi K, Morita M, Yoshioka M, Inoue K. Cardiovascular dysautonomia in de novo Parkinson's disease. J Neurol Sci 2006;241:59–65.

[10] Zakrzewska-Pniewska B, Jamrozik Z. Are electrophysiological autonomic tests useful in the assessment of dysautonomia in Parkinson's disease? Parkinsonism Relat Disord 2003;9:179–83.

[11] Goldstein DS. Dysautonomia in Parkinson's disease: neurocardiological abnormalities. Lancet Neurol 2003;2:669–76.

[12] Goldstein DS, Eldadah BA, Holmes C, Pechnik S, Moak J, Saleem A, et al. Neurocirculatory abnormalities in Parkinson's disease with orthostatic hypotension: independence from Levodopa treatment. Hypertension 2005;46:1333–9.

[13] Mihci E, Kardelen F, Dora B, Balkan S. Orthostatic heart rate variability analysis in idiopathic Parkinson's disease. Acta Neurol Scand 2006;113:288–93.

[14] Hughes AJ, Daniel SE, Kilford L, Lees AJ. Accuracy of clinical diagnosis of idiopathic Parkinson's disease: a clinico-pathological study of 100 cases. J Neurol Neurosurg Psychiatry 1992;55:181–4.

[15] Wheeler T, Watkins PJ. Cardiac denervation in diabetes. Br Med J 1973;4:584–6.

[16] Task Force of the European Society of Cardiology and the North American Society of Pacing and Electrophysiology. Heart rate variability: standards of measurement, physiological interpretation, and clinical use. Heart J 1996;17:354–81.

[17] Senard JM, Rai S, Lapeyre-Mestre M, Brefel C, Rascol O, Rascol A, et al. Prevalence of orthostatic hypotension in Parkinson's disease. J Neurol Neurosurg Psychiatry 1997;63:584–9.

[18] Ponsen MM, Stoffers D, Booij J, van Eck-Smit BL, Wolters ECh, Berendse HW, et al. Idiopathic hyposmia as a preclinical sign of Parkinson's disease. Ann Neurol 2004;56:173–81.

[19] Goldstein DS, Holmes C, Li ST, Bruce S, Metman VL, Cannon RO. Cardiac sympathetic denervation in Parkinson's disease. Ann Intern Med 2000;133:338–47.

[20] Goldstein DS, Holmes CS, Dendi R, Bruce SR, Li ST. Orthostatic hypotension from denervation in Parkinson's disease. Neurology 2002;58:1247–55.

[21] Kallio M, Haapaniemi T, Turkka J, Suominen K, Tolonen U, Sotaniemi K, et al. Heart rate variability in patients with untreated Parkinson's disease. Eur J Neurosci 2000;7:667–72.

[22] Zakrzewska-Pniewska B, Jamrozik Z. Are electrophysiological autonomic tests useful in the assessment of dysautonomia in Parkinson's disease? Parkinsonism Relat Disord 2003;9:179–83.

[23] Lu SF, Young HJ, Lin MT. Nigrostriatal dopamine system mediates baroreflex sensitivity in rats. Neurosci Lett 1995;190:17–20.

[24] Haensch CA, Jörg J. Beat-to-beat blood pressure analysis after premature ventricular contraction indicates sensitive baroreceptor dysfunction in Parkinson's disease. Mov Disord 2006;21:486–91.

[25] Benarroch EE, Schmeichel AM, Parisi JE. Preservation of brachiomotor neurons of the nucleus ambiguus in multiple system atrophy. Neurology 2003;60:115–7.

[26] Benarroch EE, Schmeichel AM, Sandroni P, Low PA, Parisi JE. Involvement of vagal autonomic nuclei in multiple system atrophy and Lewy body diseases. Neurology 2006;66:378–83.

[27] Izzo PN, Deuchars J, Spyer KM. Localization of cardiac vagal preganglionic motoneurones in the rat: immunohistochemical evidence of synaptic inputs containing 5-hydroxytryptamine. J Comp Neurol 1993;327:572–83.

[28] Cheng Z, Powley TL. Nucleus ambiguus projections to cardiac ganglia of rat atria: an antegrade tracing study. J Comp Neurol 2000;424:588–606.

[29] Iwanaga K, Wakabayashi K, Yoshimoto M, Tomita I, Satoh H, Takashima H, et al. Lewy body-type degeneration in cardiac plexus in Parkinson's and incidental Lewy body disease. Neurology 1999;52:1269–71.

[30] Okada Y, Ito Y, Aida J, Yasuhara M, Ohkawa S, Hirokawa K, et al. Lewy bodies in the sinoatrial nodal ganglion: clinicopathological studies. Pathol Int 2004;54:682–7.

[31] Haensch CA, Lerch H, Jörg J, Isenmann S. Cardiac denervation occurs independent of orthostatic hypotension and impaired heart rate variability in Parkinson's disease. Parkinsonism Relat Disord 2008, doi:10.1016/j.parkreldis.2008.04.031.

Clinical utility of anti-signal recognition particle antibody in the differential diagnosis of myopathies

S. Suzuki[1], T. Satoh[2], S. Sato[2], M. Otomo[3], Y. Hirayama[4], H. Sato[1], M. Kawai[3], T. Ishihara[5], N. Suzuki[1] and M. Kuwana[2]

Objective. Auto-antibodies to signal recognition particle (SRP) are known to be specific to PM among rheumatic disorders, but the specificity in myopathic diseases remains unclear. The clinical utility of anti-SRP antibody in the differential diagnosis of myopathies has not been studied. The aim of the present study was to elucidate whether detection of anti-SRP antibody can discriminate of PM from muscular dystrophy (MD).

Methods. We report a patient with a childhood onset myopathy, in whom it was clinically difficult to make a differential diagnosis of PM or MD for 21 yrs, despite repeated muscle biopsies. Myositis-specific auto-antibodies to RNA-associated antigens were screened in this particular case as well as in 105 serum samples from various types of MD and 84 from PM patients using RNA immunoprecipitation. The MD and PM serum samples were obtained from different institutions. The presence of anti-SRP antibody was confirmed by RNA immunoprecipitation combined with immunodepletion of SRP from the antigen.

Results. Anti-SRP antibody was positive in the present patient, supporting the diagnosis of PM. Anti-SRP antibody was detected in seven (8.3%) patients with PM, but in none of the patients with MD. Myositis-specific auto-antibodies were not detected in any of the patients with MD.

Conclusion. Anti-SRP antibody is useful for discriminating PM from MD among patients with myopathies.

KEY WORDS: Anti-signal recognition particle antibody, Polymyositis, Muscular dystrophy.

Introduction

The inflammatory myopathies are a heterogeneous group of systemic diseases characterized by muscle weakness, elevated serum creatine kinase (CK) values, electromyographic abnormalities and inflammatory infiltrates in skeletal muscle [1]. Myositis-specific auto-antibodies include those directed against aminoacyl-tRNA synthetases (ARS), signal recognition particle (SRP) and nuclear helicase Mi-2. Anti-Jo-1 antibody, one of the anti-ARS antibodies, is closely related to PM and DM with a high frequency of intestinal lung disease (ILD) [2]. On the other hand, anti-SRP antibody is clinically associated with pure PM [3–6]. SRP, one of the most abundant and best characterized RNP particles, regulates the translocation of proteins across the endoplasmic reticulum during protein synthesis [3, 4]. Patients with anti-SRP antibodies most often present with severe muscle involvement characterized by rapidly developing proximal weakness that culminates in severe disability, and often by a poor response to steroid therapy [6].

Muscular dystrophy (MD), a group of hereditary and sporadic progressive diseases, each with unique phenotypic and genetic features, is the most common and representative myopathy [7]. It is sometimes difficult to distinguish anti-SRP-positive PM patients from MD patients for the following reasons [8]. First, since anti-SRP-positive PM patients have a low incidence of pulmonary fibrosis, skin rash, arthritis and RP, it is difficult to differentiate them from MD patients based on the clinical manifestations alone.

Second, severe necrosis of skeletal muscle without lymphocytic infiltration is a histological finding common to both anti-SRP-positive PM and MD [9, 10]. In similar clinical settings, it has not been elucidated whether the detection of auto-antibodies using RNA immunoprecipitation is reliable for the differential diagnosis of myopathies, especially between MD and PM. To address this question, we screened the serum of MD patients and PM patients for myositis-specific auto-antibodies, including anti-SRP antibody.

Patients, materials and methods

Case report

A 32-yr-old Japanese man was admitted to Keio University Hospital in 2004 for evaluation of long-standing myopathy. He had a 21-yr history of severe weakness in the trunk, arms and legs, but no familial history of neuromuscular disorders. He was normal until the age of 10 yrs of age, when he had difficulty in running fast and hanging from a horizontal bar. When he first visited the other hospital at age 11 yrs, he showed scapulohumeral dominant muscle atrophy without facial muscle involvement. Serum CK was 4180 IU/l (normal, <198 IU/l), and the electromyography showed myopathic features. The first muscle biopsy of the left biceps brachii muscle revealed a prominent variation in muscle fibre size, but no perifascicular atrophy. Necrotic muscle fibres were observed with evidence of regeneration, but there was no lymphocytic infiltration in the perimysial or perivascular region. Endomysial connective tissue was increased (Fig. 1A and B). Under the tentative diagnosis of scapulohumeral MD, oral predonisolone (1 mg/kg/day) therapy was prescribed for 3 months, but the patient did not respond to the treatment. His weakness worsened over the next 2 yrs, and he eventually lost ambulation and had difficulty in blowing, swallowing and eating at the age of 13 yrs. After the bulbar symptoms continued for ~6 months, his symptoms gradually began to improve. However, he could not walk and required a wheelchair. The serum CK levels decreased to 1640 IU/l at the age of 14 yrs and 614 IU/l at the age of 16 yrs. The second muscle biopsy of the quadriceps femoris muscle was performed at 16 yrs of age. The muscle fibres had largely been

[1]Department of Neurology, [2]Division of Rheumatology, Department of Internal Medicine, Keio University School of Medicine, Tokyo, [3]Department of Neurology, Higashisaitama National Hospital, Saitama, [4]Department of Pediatric Neurology, Tokyo Metropolitan Higashiyamato Medical Center for the Severely Disabled, Tokyo and [5]Department of Neurology, Hakone National Hospital, Kanagawa, Japan.

1539

S. Suzuki *et al.*

replaced by adipose tissue, but there still was no lymphocytic infiltration (Fig. 1C). There have been no changes in his muscle weakness since then.

The neurological examination on admission revealed severe symmetrical proximal-dominant weakness, with Medical Research Council scale grade at 3/5 in the lower extremities and 4/5 in the upper extremities, but there was no facial muscle involvement. Muscle atrophy was remarkable in the lower trunk and proximal muscles of the legs. Deep tendon reflex was absent. The CK levels had retuned to the normal range. T_1-weighted muscle magnetic resonance images of the thighs showed evidence of severe diffuse muscle atrophy.

Patients and sera

Serum samples were obtained from *the patient* described above, and from 105 Japanese patients with MD (82 males and 23 females) who were seen consecutively between January 2005 and June 2006 at Higashisaitama National Hospital. The mean age of the MD patients at the time of serum collection was 30.3 ± 17.2 yrs. The MD cases included those with Duchenne MD ($n = 58$), Becker MD ($n = 6$), myotonic MD ($n = 19$), limb-girdle MD ($n = 6$), faciosca-pulohumeral MD ($n = 4$), Fukuyama-type congenital MD ($n = 7$) and unclassified types of MD ($n = 5$), and the diagnosis of each was

based on clinical, pathological and genetic features [7]. In contrast, stored serum for a cohort of 84 Japanese patients with PM (25 males and 59 females) was available at Keio University Hospital. All sera were obtained at diagnosis before initiation of immuno-suppresive therapy. The mean age of the PM patients at the time of serum collection was 51.4 ± 13.4 yrs. The diagnosis of probable or definite PM was based on the criteria of Bohan and Peter [11]. Patients with DM, IBM and overlap syndrome were excluded from study entry. We obtained MD and PM serum samples from different institutions because most MD patients, especially those with Duchenne MD, stayed at the national hospital and sanatorium for the severely disabled. All blood samples and clinical information were obtained after patients provided informed consent and ethical approval. The study was approved by the institutional review boards.

RNA immunoprecipitaion

RNA immunoprecipitation assay was performed using extracts from leukaemia cell line K562, as previously described [12]. Briefly, a 10 μl volume of patient serum was mixed with 2 mg of protein A-Sepharose CL-4B (Pharmacia Biotech AB, Uppsala, Sweden) in 500 μl of immunoprecipitation buffer (10 mM Tris-HCl, pH 8.0, 500 mM NaCl, 0.1% Nonidet P40), and after incubation for 2 h, was washed three times with immunoprecipita-tion buffer. Antibody-bound Sepharose beads were mixed with 100 μl of K562 cell extract (6 × 10^6 cell equivalents per sample) for 2 h, and 30 μl of 3 M sodium acetate, 30 μl of 10% SDS and 300 μl of phenol:chloroform:isoamyl alcohol (50:50:1, containing 0.1% 8-hydroxyquinoline) were added to extract bound RNA. After ethanol precipitation, the RNA was resolved on a 7 M urea–10% polyacrylamide gel, and the gel was silver-stained (Bio-Rad, Hercules, CA, USA).

Immunodepletion experiments

The immunodepletion studies were undertaken using prototype sera obtained from two anti-SRP-positive PM patients (patients #1 and #2). A 50 μl volume of the prototype serum #2 and normal serum as a negative control was mixed with 10 mg of protein A-Sepharose CL-4B in 500 μl of immunoprecipitation buffer, and incubated for 2 h. After washing three times with immunopreci-pitation buffer, the antibody-bound Sepharose beads were mixed with 100 μl of K562 cell extract for 2 h to fully the deplete antigens recognized by prototype serum #2 or normal serum. Then, the supernatant was further incubated with Sepharose beads pre-conjugated with the present patient serum and the prototype serum #1. After washing for five times, the RNA immunopreci-pitation assay was analysed as described above.

Statistic analysis

The frequencies of MD patients and PM patients who were positive for each auto-antibody were compared. Categorical variables were compared by the χ^2-test.

Results

Our patient's serum immunoprecipitated RNA located in the 7S RNA lesion, as did the prototype serum #1 obtained from an anti-SRP-positive PM patient (Fig. 2, lanes 2 and 5). Immunodepletion treatment with the other prototype #2 serum obtained from an anti-SRP-positive PM patient successfully depleted the SRP-antigen complex from the extract (lane 3), but normal serum did not (lane 4). Immunoprecipitation of 7S RNA in our patient was cancelled when SRP-antigen depleted extract was used (lane 6). These findings confirmed that our patient's serum was positive for anti-SRP antibody.

We screened auto-antibodies to RNA-associated auto-antigens in sera from 105 MD patients and 84 PM patients by the RNA
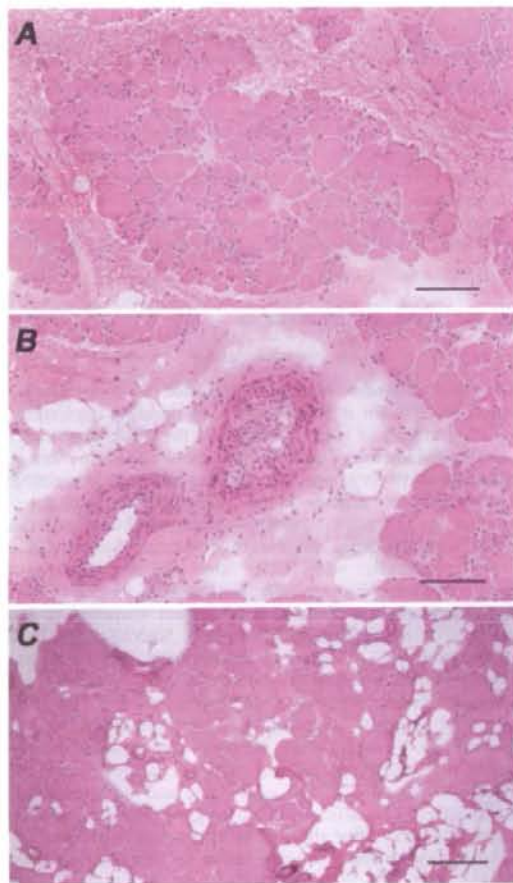

Fig. 1. Histological findings of the present patient. The histological appearance of muscle biopsy specimens obtained at 11 yrs of age (**A** and **B**) and 16 yrs of age (**C**). Haematoxylin–eosin staining. Bar = 100 μm.

immunoprecipitation assay. The frequencies of myositis-specific auto-antibodies detected by RNA immunoprecipitation in MD patients and PM patients are summarized in Table 1. Anti-SRP antibodies were detected in 7 PM patients (8.3%), but in none of the MD patients ($P = 0.008$). Similarly, auto-antibodies to ARS, such as those to Jo-1, PL-7, PL-12, EJ and OJ, were detected in PM patients, but not in MD patients. Myositis-specific auto-antigens were not detected in MD patients.

Table 2 shows the clinical and histological findings of the present case and for seven PM patients with anti-SRP antibodies. The eight PM patients with anti-SRP antibodies had common clinical features including muscle weakness, levels of serum

CK > 3000 IU/l (except for one case) and myopathic findings in the EMG. Although three patients had ILD, none had skin rash, arthritis or RP. Malignancy was found in two patients. Response to high-dose steroid therapy was generally poor. Most patients showed refractory muscle weakness and required other immuno-suppressive agents. Histological findings disclosed severe necrosis with regeneration of skeletal muscle in all patients, and lymphocytic infiltration in half.

Discussion

In this article, we describe a case of myopathy with childhood onset, in whom it was difficult to make a differential diagnosis between PM and MD despite repeated muscle biopsy. The patient was found to be positive for anti-SRP antibody 21 yrs after onset. Screening the serum of MD patients and PM patients by RNA immunoprecipitation assay for auto-antibodies revealed anti-SRP antibodies in seven (8.3%) PM patients, but not in MD patients. However, the comparison of frequencies of these auto-antibodies may not be appropriate, since the MD and PM patients were selected from medical centres with different settings. Anti-SRP antibody was found to be specific to PM and useful in excluding MD in patients with myopathies.

Anti-SRP antibody was detected in 8.3% in our cohort of Japanese PM patients, similar to the rate in European patients [13]. Although anti-SRP antibody is known to be PM-specific, it has also been found in patients with DM, IBM and SSc [6, 13]. However, the specificity of anti-SRP antibody in myopathic diseases is not fully elucidated. Perurena et al. [14] and Hengstman et al. [15] reported that anti-SRP antibody was negative in 17 and 48 patients with MD, respectively. Combining these results with our findings, anti-SRP antibody is not exclusively present in a total of 170 patients with MD. These findings suggest that production of anti-SRP antibody does not result from non-specific muscle injuries.

Although muscle biopsy is the most accurate method of establishing a diagnosis of PM, but its interpretation is sometimes difficult [1]. van der Meulen et al. [16] have reported that PM is an overdiagnosed entity using strict diagnostic criteria of muscle biopsy. To avoid misdiagnosis of PM, Dalakas and Hohlfeld [1]
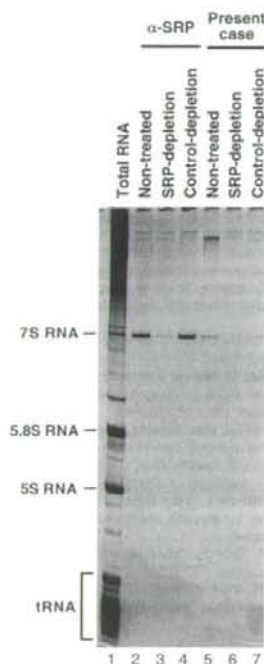

Fig. 2. Analysis of immunoprecipitates from K562 cell extracts by 7 M urea–10% PAGE and silver staining. The results of the prototype serum #1 of the anti-signal recognition particle (SRP)-positive PM patient (lanes 2–4) and the present patient serum (lanes 5–7) are compared. Immunoprecipitates were obtained from no treatment (lanes 2 and 5), after immunodepletion using prototype serum #2 from an anti-SRP-positive patient (lanes 3 and 6), and serum from a healthy control (lanes 4 and 7).

TABLE 1. Frequencies of myositis-specific auto-antibody detection by RNA immunoprecipitation in patients with MD and those with PM

Auto-antibodies	MD ($n = 105$)	PM ($n = 84$)	P-value
Anti-SRP, n (%)	0	7 (8.3)	0.008
Anti-ARS (anti-Jo-1), n (%)	0	17 (20.2)	<0.0001
Anti-ARS (non-anti-Jo-1), n (%)	0	10 (11.9)[a]	0.0009

[a]Auto-antibodies to PL-7 were found in three, PL-12 in two, EJ in four, and OJ in one.

TABLE 2. Clinical and histological findings from PM patients with anti-SRP antibodies

Findings	Presen case	#1	#2	#3	#4	#5	#6	#7
Onset age/gender	11/M	39/M	41/F	48/F	53/F	55/M	66/M	82/M
Muscle weakness	(+)	(+)	(+)	(+)	(+)	(+)	(+)	(+)
Muscle atrophy	(+)	(−)	(−)	(−)	(−)	(−)	(−)	(+)
ILD	(−)	(+)	(+)	(−)	(−)	(−)	(+)	(−)
DM rash	(−)	(−)	(−)	(−)	(−)	(−)	(−)	(−)
Arthritis	(−)	(−)	(−)	(−)	(−)	(−)	(−)	(−)
RP	(−)	(−)	(−)	(−)	(−)	(−)	(−)	(−)
CK (IU/l)	4180	6400	569	3670	6471	3477	8594	15 880
Myopathic change in EMG	(+)	(+)	(+)	(+)	(+)	(+)	(+)	(+)
Malignancy	(−)	(−)	(−)	(−)	(+)	(−)	(−)	(+)
Treatment response	None	Partial	Partial	None	Partial	Partial	Partial	Partial
Muscle biopsy								
Small size of myofibre	(+)	(+)	(+)	(+)	(+)	(+)	(+)	(+)
Lymphocyte infiltration	(−)	(+)	(−)	(+)	(+)	(−)	(+)	(−)
Necrosis	(+)	(+)	(+)	(+)	(+)	(+)	(+)	(+)
Regeneration	(+)	(+)	(+)	(+)	(+)	(+)	(+)	(+)
Perifascular atrophy	(−)	(−)	(−)	(−)	(−)	(−)	(−)	(−)